Introduction

The multidrug resistance-associated protein 2 (MRP2) or canalicular multispecific organic anion transporter (cMOAT) is a 190–200 kDa transmembrane glycoprotein comprised of 1545 amino acids and belongs to the superfamily C of ATP-binding cassette (ABC) transporters. This transporter is expressed on hepatic canalicular membranes, intestinal apical membranes, luminal membranes of renal proximal tubules, placental epithelial cells, and the blood brain barrier.[1] MRP2 exports endogenous and exogenous substances, preferentially organic anions or conjugates with glucuronide, glutathione and sulfate.[1-3] This protein originally identified in cisplatin-resistant tumor cells[4] is shown to confer drug resistance to other anti-cancer drugs, such as vincristine and doxorubicin.[5,6]

MRP2 is encoded by the *ABCC2* gene located on chromosome 10q24 and consists of 32 exons (31 coding exons) and spans 69 kb. Several *ABCC2* genetic variations have been detected in patients with Dubin-Johnson syndrome (DJS), an autosomal recessive disease characterized by hyperbilirubinemia with conjugated bilirubin or increased coproporphyrin excretion in urine.[2,7] Recent studies on *ABCC2* have identified common single nucleotide polymorphisms (SNPs) such as −24C>T and −3972C>T (Ile 1324Ile) among several ethnic populations, and several studies have suggested their association with altered MRP2 expression or function.[8-17] In more recent studies on *ABCC2* haplotypes covering an extended 5′-flanking region, close linkages were found among −1549A>G in the 5′-flanking region and two common SNPs −24C>T and −3972C>T (Ile1324Ile).[8] In addition, as possible functional SNPs, −1774delG in Koreans[8] and −1019A>G in Caucasians[10] were reported. However, there is little information on detailed haplotype structures throughout the gene, and comprehensive haplotype analysis in Japanese has not yet been conducted.

We previously analyzed *ABCC2* genetic variations within all 32 exons and the proximal 5′-flanking region (approximately 800 bp upstream of the translation initiation site) using established cell lines derived from Japanese cancer patients to obtain preliminary information on *ABCC2* SNPs in Japanese.[18] In this study, to reveal *ABCC2* haplotype structures in Japanese, we resequenced the *ABCC2* gene including the distal 5′-upstream region (approximately 1.9 kb upstream from the translation initiation site) as well as all 32 exons in 236 Japanese subjects and conducted haplotype analysis using the detected genetic polymorphisms.

Materials and Methods

Human DNA samples: Genomic DNA samples were obtained from blood leukocytes of 177 Japanese cancer patients at two National Cancer Center Hospitals (Tokyo and Chiba, Japan) and Epstein-Barr virus-transformed lymphoblastoid cells prepared from 59 healthy Japanese volunteers at the Tokyo Women's Medical University under the auspices of the Pharma SNP consortium (Tokyo, Japan). Written informed consent was obtained from all subjects. Ethical review boards of all participating organizations approved this study.

PCR conditions for DNA sequencing: We sequenced all 32 exons of the *ABCC2* gene and approximately 800 bp upstream of the translation initiation codon (proximal 5′-flanking region) as described previously and also extended the sequenced region to 1.9 kb upstream of the translation initiation site (distal 5′-flanking region). Briefly, for amplification of the proximal 5′-flanking region and 32 exons, 5 sets of multiplex PCR were performed from 200 ng of genomic DNA using 1.25 units of Z-taq (Takara Bio. Inc., Shiga, Japan) with 0.3 uM each of the mixed primers as shown in **Table 1** [1st PCR]. The first PCR conditions consisted of 30 cycles of 98°C for 5 sec, 55°C for 5 sec, and 72°C for 190 sec. Next, each exon was amplified separately using the 1st PCR product by Ex-Taq (0.625 units, Takara Bio. Inc.) with appropriate primers (0.3 uM) (**Table 1**) [2nd PCR]. The conditions for the second round PCR were 94°C for 5 min, followed by 30 cycles of 94°C for 30 sec, 55°C for 1 min, and 72°C for 2 min, and then a final extension at 72°C for 7 min. For amplification of the distal 5′-flanking region, multiplex PCR was performed from 25 ng of genomic DNA using 1 unit of Ex-Taq (Takara Bio. Inc.) with 0.4 uM each of the 2 sets of primers as shown in **Table 1** [PCR]. The PCR conditions were 94°C for 5 min, followed by 30 cycles of 94°C for 30 sec, 60°C for 1 min, and 72°C for 2 min, and then a final extension at 72°C for 7 min.

Following the PCR, products were treated with a PCR Product Pre-Sequencing Kit (USB Co., Cleveland, OH, USA) and directly sequenced on both strands using an ABI BigDye Terminator Cycle Sequencing Kit (Applied Biosystems, Foster City, CA, USA) with the sequencing primers listed in **Table 1** (Sequencing). Excess dye was removed by a DyeEx-96 kit (Qiagen, Hilden, Germany), and the eluates were analyzed on an ABI Prism 3700 DNA Analyzer (Applied Biosystems). All variations were confirmed by sequencing PCR products generated from new amplifications from genomic DNA. Genbank NT_030059.12 was used as the reference sequence.

Linkage disequilibrium (LD) and haplotype analyses: Hardy-Weinberg equilibrium and LD analyses were performed using SNPAlyze 3.1 software (Dynacom Co., Yokohama, Japan). Pairwise LDs were shown as rho square (r^2) and $|D'|$ values in **Figure 1**. Diplotype configurations (haplotype combinations) were inferred by LDSUPPORT software, which determined the posterior probability distribution of diplotype configurations for each subject based on estimated haplotype frequencies[19].

Results and Discussion

In this study, sixty-one *ABCC2* genetic variations including 36 novel ones were detected in 236 Japanese subjects

Table 1. Primer sequences used in this study

Amplified or sequenced region	Forward primer (5′ to 3′)	Reverse primer (5′ to 3′)	Amplified region[a]
PCR (Ex-taq)			
5′-Flanking (for −1.9 k to −1.7 k)	CCACCAGTGCCAAGAGAAGTAT	CACAAGTCATCTGGAAAACACA	20289134–20289443
5′-Flanking (for −1.7 k to −950)	ATGAGGTGGTATCTAACTGTGG	AAATGTTTTCTGTAGGGACGGG	20289392–20290182
1st PCR (Z-taq)			
5′-Flanking (for −1.2 k) to exon 6	ATACTGCATGGGTGGTTATG	AACCTGCCTCCAAATTTTTC	20289942–20303347
Exons 7 to 11	GGAGAATCACTTTGAAGCCG	CTAGCAAGTGTGAGGGGTGT	20304874–20314079
Exons 12 to 19	TCTGTGAATGTGGCAAAACT	GGATCTACCAAGAATTTAGC	20315189–20328004
Exons 20 to 25	GATGAGCATTTTCAATTTAC	TCAGTTCACCCAGCACTTAT	20338211–20344941
Exons 26 to 32	GAGCAAGACCTTGTCTCATA	CCATGGATGAATCTCAGATA	20349821–20360334
2nd PCR (Ex-taq)			
5′-Flanking (for −880 to −130)	GGAAGATCGCTTGAACCCAT	TCATCCCAACCATTTAATCG	20290245–20290994
Exon 1	TTGTTGGCCAGCTCTGTTG	TTCTGGTTCTTGTTGGTGAC	20290810–20291254
Exon 2	GGGTAAGGCTGGATATGGAT	CTGGCTCTACCTGAGACAAT	20292767–20293194
Exon 3	CACCGGAAACCATTCTGTTC	TTTGCCTCACTATGGATCCC	20300442–20300773
Exon 4	GCCAGATTAGTCACGACAGT	CCAAAGGAAGTCTACATGGCC	20301708–20302134
Exon 5	CAGGTAAGGAAAAAAAGAGTGG	CCTTGTCATAAAATGGTCTG	20301966–20302418
Exon 6	TATGCCAGAAAATCTGATTA	AGGTGGAACATGAGCTTGAGT	20302499–20303070
Exon 7	GGTGGAGATAGCCTCTGACC	TGCACTGAGAAGTATGAAGTGC	20305320–20305728
Exon 8	CCTGTACAGAGAAGGCCACG	TGCGGTCTTCATGAACACAA	20307385–20307816
Exon 9	GGCTTTGGACAATTCTGGTC	TCCACCCATTGTCTGTGAAC	20308539–20309038
Exon 10	AGGCAAGAAGTCACAGTGCC	TTGCCCAAACTCCCATTAAG	20312158–20312650
Exon 11	ACAGTCAGGCAAGGGCTATG	GACAGGAGGACATGAAACAA	20313420–20313873
Exon 12	GATTTCTATTCCCCACATTT	GAGCTGGGGGTATGGTACAA	20315554–20315983
Exon 13	GTGACCTTGGAGAAGATATT	CTCTTGAAAGTTTACCAGCA	20316189–20316623
Exon 14	TTGCTCAAGGACTGAAATAG	CCTGCTTATCCTCAGAAGAG	20318223–20318732
Exon 15	GGTCTCATGGTCTCATTCTA	GGGTTTATCCTGCACTAGTA	20319650–20320025
Exon 16	AGAAGCACTTTGGGGTCTTGTA	GCTGAAATGGGAAGGAGAATC	20321144–20321581
Exon 17	GCTGAAAAACGATAGTCCAA	TCAACTAGATTACCCCTGTGT	20325354–20325863
Exons 18 and 19	TCACAGGGTGACAAGCAAC	TTGAATCTCTGGGTAGTTTG	20326820–20327678
Exon 20	GAAACCAGCAAGATCAGAGGA	TCACTCAGCTGGCATCAAAG	20338493–20338929
Exon 21	TGACTGTGACATCTGCTTGC	GGACAGAGGACATATTGCTCC	20338927–20339248
Exons 22 and 23	GCATTGTATTTCAGCATTGT	ACAGTGTTGTCTAGGGGGAC	20339701–20340506
Exon 24	GAACACACAGAATCCAACAGA	TCACTTCAGCTTCAGACAGT	20342562–20343001
Exon 25	TCTCATTGGTCTCCTCCTCG	AATTTCACACCACTAGCCAT	20344186–20344672
Exon 26	GAGGCATTGCCTAAGAGTGC	AAAGATGGAGCCAGGGTTTG	20350122–20350523
Exons 27 and 28	GGCAAGGATTGTCTTTCTTA	CGACAGCTGCGGTAAGTCTG	20351928–20352954
Exon 29	AGAGATGGAGTAGCCAGTCAC	CAGCCACAAATGCATATTACC	20353790–20354262
Exon 30	GAAGCTCAACCACAAACCAG	GCTCGACCAGTTTTCAAGAG	20355106–20355610
Exon 31	GCAAGGTACAGCTAGTTGAA	GCGTGATGTAAAATTTTGGC	20358730–20359248
Exon 32	GCTGTGGCTCATTGATTTTC	AAGGTGATAAAACAGAAATG	20359651–20360213
Sequencing			
5′-Flanking (for −1.7 k)	CCACCAGTGCCAAGAGAAGTAT	CACAAGTCATCTGGAAAACACA[b]	
(for −1.7 k to −1.3 k)	GGTATCTAACTGTGGTTTTG	GAAGGAAAGGAGTCAAAGGAAC	
(for −1.5 k to −950)	TCCCACACTGAATGCTGCCTTT	TAGGGACGGGGTCTCACTAT	
(for −880 to −400)	GGAAGATCGCTTGAACCCAT[b]	ATGTGCAGTTTCGCTTCTG	
(for −570 to −130)	CATATAGGCTCACACTGGAT	TCATCCCAACCATTTAATCG[b]	
Exon 1	TGGTTCCTTTTATGTATGGC	GTTCTTGTTGGTGACCACCC	
Exon 2	AAAGCAGTGGGATGTGCTG	TGTCTCTACTGTGCACCAAGG	
Exon 3	CACCGGAAACCATTCTGTTC[b]	TTTGCCTCACTATGGATCCC[b]	
Exon 4	CCTCCTTTCTTCCCATGTTC	CTCAACTTGATGCCATTTAC	
Exon 5	TGGGGCAACCTCTAACTCATA	TGAGACCCAGACATCTTAAA	
Exon 6	TTAGGGTCTCCAAATAAACA	ACTTTCAGAGGAGTGAGAGAGT	
Exon 7	GGTGGAGATAGCCTCTGACC[b]	TGCACTGAGAAGTATGAAGTGC[b]	
Exon 8	CCTGTACAGAGAAGGCCACG[b]	CACAATGCTGTAAGGTTAAG	
Exon 9	GGCTTTGGACAATTCTGGTC[b]	TCCACCCATTGTCTGTGAAC[b]	
Exon 10	GTGCCTTGGAGAAGCTGTGT	TTGCCCAAACTCCCATTAAG[b]	
Exon 11	TCACTGGGCACCTCAAGTTC	GGAATCCATCACCTCTACCA	
Exon 12	ACATTTTGGGGACTATATCT	ATGCCAGCTAGTCTATCAAA	
Exon 13	GGAGGCTGGATGATCCTTAAG	CTCTTGAAAGTTTACCAGCA[b]	
Exon 14	CATCTGTCTATGGTGGGATA	ATAGGCTCAAGACAAATCTC	
Exon 15	GATTTCATTCACCTCCTGTT	CATTTCCCCATGCATTCTAT	
Exon 16	CCAATCTTGAGGGGAAATCT	TCCAAGACCTCACCTACTAGC	

Table 1. continued

Amplified or sequenced region	Forward primer (5′ to 3′)	Reverse primer (5′ to 3′)	Amplified region[a]
Exon 17	GTGGAATAACTACAAGCACG	TCAACTAGATTACCCCTGTGT[b]	
Exon 18	GGTGACAAGCAACAAAACTA	CCACCATCTTCCCTGTCTTA	
Exon 19	GATGCTCATGTAGGAAAACA	TTTACCATTCCACCCATGGC	
Exon 20	GGCTTCTCTCTCCTTGTTCA	CAAAGAAACAAAGGAAGAGC	
Exon 21	TGACTGTGACATCTGCTTGC[b]	GGACAGAGGACATATTGCTCC[b]	
Exon 22	GCATTGTATTTCAGCATTGT[b]	GATATTTGATGCATGGACGA	
Exon 23	GAATCTGTCTGGACCCTGTA	GTCTAGGGGGACATAATAAT	
Exon 24	ACACACAGAATCCAACAGAT	TCAACATATGACTAAATGGC	
Exon 25	GGAGCCTCTCATCATTCTGC	TTTCACACCACTAGCCATGC	
Exon 26	CCGATCAAGTCAAACCCTCT	TTTGAACCTCAGTCTTCTTT	
Exon 27	TTTCCTTACTCCCTTGTAGA	AAACTTTAGGGACCCATTAT	
Exon 28	CTGCTACCCTTCTCCTGTTC	CCTTCCCTCTGATACTGTGT	
Exon 29	TACCTCCTGTGACTGTGAAT	CAGCCACAAATGCATATTACC[b]	
Exon 30	GCCAGTCCTATCCACCATCT	AACACGAGGAACACGAGGAG	
Exon 31	GATCTGGAACATGAAAATGG	TTTTGGCCAGATTACTTGAC	
Exon 32	GCTCATTGATTTTCACTGCT	AAGGCAAAGGAATAATTATCG	

[a]The reference sequence is NT_030059.12.
[b]The same primer that was used for the 2nd PCR.

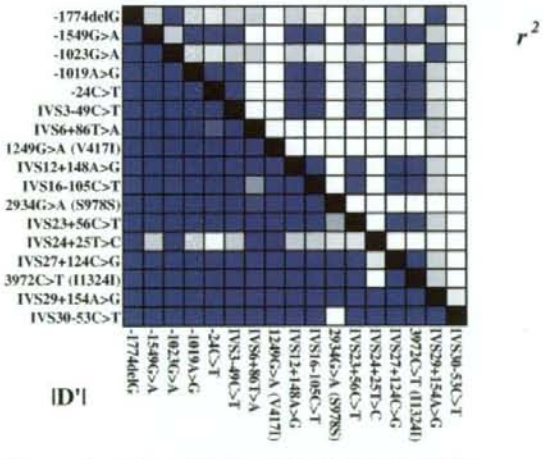

Fig. 1. Linkage disequilibrium (LD) analysis of *ABCC2*
Pairwise LD (r^2 values and |D′|) of polymorphisms detected in no less than 3% of allele frequencies is shown as a 10-graded blue color.

(**Table 2**). All detected variations were in Hardy-Weinberg equilibrium ($p > 0.05$). Novel variations consisted of 5 non-synonymous and 4 synonymous variations in the coding region, 22 in the intronic regions, 3 in the 5′-flanking region, 1 in the 3′- flanking region, and 1 in the 3′-UTR. The novel non-synonymous variations were 1177C>T (Arg393Trp), 1202A>G (Tyr401Cys), 2358C>A (Asp786Glu), 2801G>A (Arg934Gln), and 3320T>G (Leu1107Arg), and their frequencies were 0.002. No statistically significant differences were found in the allele frequencies of all variations between 177 cancer patients and 59 healthy subjects ($P > 0.05$, Fisher's exact test), although a larger number of subjects would be needed to conclude.

The frequency of the known common SNP −24C>T (0.173) was comparable to those reported in Asians (0.17–0.25)[8,12,20] and Caucasians (0.15–0.23)[9,10,14,15,21]. The allele frequency of another common SNP, 3972C>T (Ile1324Ile) (0.216), was also comparable to those in Asians (0.22–0.30)[8,12,20] but lower than those in Caucasians (0.32–0.37)[9,10,14,15,21]. The other major variations in the 5′-flanking region, −1774delG and −1549G>A, were found at frequencies of 0.343 and 0.203, respectively, and these values were similar to those obtained in Koreans (0.34 and 0.21, respectively).[8] However, the relatively frequent SNPs 1446C>G (Thr482Thr) (allele frequency = 0.125), IVS15-28C>A (0.333) and IVS28+16G>A (0.167) in Caucasians[17] were not detected in our study.

The LD profile of the *ABCC* variations (no less than 3% allele frequency) is shown in **Figure 1**. As assessed by r^2 values, close linkages were observed among −1774delG, −1023G>A and IVS29+154A>G, and among −1549G>A, −1019A>G, −24C>T, IVS3-49C>T, IVS12+148A>G, IVS15+169T>C, IVS16-105C>T, IVA23+56C>T, IVS27+124C>G, and 3972C>T (Ile1324Ile). It must be noted that complete linkage was observed between −1549G>A and −1019A>G in our population. In |D′| values, strong LD was also observed almost throughout the region analyzed. Overall, since close associations between the variations were observed throughout the entire *ABCC2* gene, the region sequenced was analyzed as a single LD block for the haplotype inference.

The *ABCC2* haplotype structures were analyzed using 61 detected genetic variations and a total of 64 haplotypes were identified/inferred. **Figure 2** summarizes the haplotypes and their grouping. Our nomenclature system is based on the recommendation of Nebert.[22] Haplotypes without

Table 2. Summary of *ABCC2* variations detected in this study

SNP ID				Position				
This Study	dbSNP (NCBI)	JSNP	Reference	Location	NT_030059.12	From the translational initiation site or from the end of the nearest exon	Nucleotide change	Amino acid change	Frequency (total = 472)
MPJ6_AC 2082			8	5′-Flanking	**20289354**	−1774	acttatcttgttG/_ttttttttttt		0.343
MPJ6_AC 2078*				5′-Flanking	**20289538**	−1590	tttaatttgttaG/Atgtatgtttgct		0.002
MPJ6_AC 2079			8, 10, 17	5′-Flanking	**20289579**	−1549	tccttatagtatG/Attgtggatatta		0.203
MPJ6_AC 2080			9, 17	5′-Flanking	**20290105**	−1023	tgggaggccaagG/Acagaaggattgt		0.343
MPJ6_AC 2081			10, 17	5′-Flanking	**20290109**	−1019	aggccaaggcagA/Gaggattgttgaa		0.203
MPJ6_AC 2028*				5′-Flanking	**20290395**	−733	acagtttctagcG/Tactgatgccacc		0.004
MPJ6_AC 2029				5′-Flanking	**20290395**	−733	acagtttctagcG/Aactgatgccacc		0.002
MPJ6_AC 2030*				5′-Flanking	**20290715**	−413	ttgcagcagaagC/Tgaaactgcacat		0.002
MPJ6_AC 2003		**ssj0000371**	9, 12, 15–18, 20, 26	Exon 1	**20291104**	−24	tagaagagtcttC/Tgttccagacgca		0.174
MPJ6_AC 2004			18	Exon 1	**20291105**	−23	agaagagtcttcG/Attccagacgcag		0.006
MPJ6_AC 2031		**ssj0000386**	17, 26	Intron 3	**20301785**	IVS3 −49	ctccccctcagtcC/Ttcggttagtggc		0.203
MPJ6_AC 2032*				Intron 6	**20302837**	IVS6 +86	tattttattattT/Attttttgagat		0.076
MPJ6_AC 2033*				Exon 7	**20305479**	732	caagtttgaaacG/Acacatgaagaga	Thr244Thr	0.002
MPJ6_AC 2066*				Intron 7	**20307421**	IVS7 −69	tcacaggctgacC/Gaccctggagctg		0.002
MPJ6_AC 2067*				Intron 7	**20307423**	IVS7 −67	acaggctgaccaC/Accctggagctgct		0.002
MPJ6_AC 2035*				Exon 9	**20308814**	1177	ggtgtaaaagtaC/Tggacagctatca	Arg393Trp	0.002
MPJ6_AC 2068*				Exon 9	**20308839**	1202	tggcttctgtatA/Gtaagaaggtaag	Tyr401Cys	0.002
MPJ6_AC 2036*				Intron 9	**20308859**	IVS9 +13	gtaagcagaataC/Tggcaggtatcac		0.002
MPJ6_AC 2037*				Exon 10	**20312319**	1227	gaccctatccaaC/Tttggccaggaag	Asn409Asn	0.002
MPJ6_AC 2009		**ssj0000388**	17, 18, 20, 23–26	Exon 10	**20312341**	1249	aaggagtacacgG/Atttggagaaacag	Val417Ile	0.097
MPJ6_AC 2010			18	Exon 10	**20312549**	1457	ccaagagtaagaC/Tcattcaggtaaa	Thr486Ile	0.019
MPJ6_AC 2069*				Intron 11	**20315600**	IVS11 −67	taaaacatgggtG/Agatcagatacac		0.002
MPJ6_AC 2038		**ssj0000390**	26	Intron 12	**20315952**	IVS12 +148	cegeeccatgccA/Gettttcctcctt		0.210
MPJ6_AC 2039*				Intron 13	**20318344**	IVS13 −73	tcatggactaacG/Aacaaagtcaaaa		0.002
MPJ6_AC 2070*				Intron 14	**20318515**	IVS14 +14	taaataaatttgG/Taagttgcttccc		0.002
MPJ6_AC 2040*				Intron 14	**20318521**	IVS14 +20	aatttggaagtt(del/ins)[a]cagcaaactga		0.002
MPJ6_AC 2071*				Intron 14	**20318594**	IVS14 +93	agcaaactgagaG/Tagagtgtggaga		0.002
MPJ6_AC 2041*				Intron 14	**20319757**	IVS14 −62	cggagagagacaC/Tgtgagggcagac		0.002
MPJ6_AC 2042*				Intron 14	**20319758**	IVS14 −61	ggagagagacacG/Atgagggcagaca		0.006
MPJ6_AC 2043		**ssj0000393**	26	Intron 15	**20320054**	IVS15 +169	aaagcaaaggttT/Ctcagccccttcc		0.210
MPJ6_AC 2044*				Intron 15	**20321170**	IVS15 −131	gtcttgtatatcC/Gaaggcaaatttt		0.004
MPJ6_AC 2045*				Intron 16	**20325422**	IVS16 −169	ttgagtcctgagA/Tgtggaataacta		0.004
MPJ6_AC 2046		**ssj0000396**	17	Intron 16	**20325486**	IVS16 −105	tgcacagttattC/Taaatttaagctc		0.214
MPJ6_AC 2072*				Exon 18	**20327159**	2358	tcttctagatgaC/Acccctgtctgca	Asp786Glu	0.002
MPJ6_AC 2012			18, 20, 23	Exon 18	**20327167**	2366	atgacccccctgtC/Ttgcagtggatgc	Ser789Phe	0.008
MPJ6_AC 2073*				Intron 19	**20327555**	IVS19 +3	gaagccacaggtA/Gtgtaagaaggat		0.002
MPJ6_AC 2047*				Intron 19	**20327645**	IVS19 +93	agtatccagtgaA/Tctagatttggaa		0.002
MPJ6_AC 2048				Intron 20	**20338745**	IVS20 +29	gctggcagccctC/Agtcagctctata		0.002
MPJ6_AC 2049*				Exon 21	**20339052**	2801	ccttgaaaactcG/Agaatgtgaatag	Arg934Gln	0.002
MPJ6_AC 2015		**ssj0000398**	8, 18, 26	Exon 22	**20339944**	2934	aggattgtttcG/Aatattcttcatc	Ser978Ser	0.040
MPJ6_AC 2050*				Exon 22	**20340061**	3051	cgactatccagcA/Gtctcagagggac	Ala1017Ala	0.002
MPJ6_AC 2051*				Exon 23	**20340337**	3181	cacaagcaactgC/Ttgaacaatatcc	Leu1061Leu	0.002
MPJ6_AC 2052		**ssj0000399**	17, 26	Intron 23	**20340470**	IVS23 +56	ggatctttctgaC/Tagggagaaatta		0.222
MPJ6_AC 2074*				Exon 24	**20342724**	3320	ttacatgcttccT/Gggggataatcag	Leu1107Arg	0.002
MPJ6_AC 2053				Intron 24	**20342843**	IVS24 +25	atggctaagtcaT/Ccettccttcctc		0.030
MPJ6_AC 2075*				Intron 24	**20342880**	IVS24 +62	agcccagcctctT/Ctcctgagaatct		0.002
MPJ6_AC 2054				Intron 24	**20342926**	IVS24 +108	cactcactcctcC/Tcctcagcagctt		0.023
MPJ6_AC 2055*				Intron 24	**20344318**	IVS24 −56	agaaaggaggaaG/Aatggtggatgcc		0.002
MPJ6_AC 2056*				Intron 26	**20352061**	IVS26 −21	atgatgatttttcA/Ggtcttctggttt		0.002
MPJ6_AC 2057*				Intron 27	**20352227**	IVS27 +44	ggcaaaaacaacA/Gtgcaactcccttc		0.008
MPJ6_AC 2058		**ssj0000404**	17, 26	Intron 27	**20352307**	IVS27 +124	aaagtttccttttC/Gctctaactcaaa		0.222
MPJ6_AC 2076			26	Exon 28	**20352688**	3927	ccaagtgcggtaC/Tcgacctgagctg	Tyr1309Tyr	0.002
MPJ6_AC 2022		**ssj0000407**	8, 12, 13, 17, 18, 20, 26	Exon 28	**20352733**	3972	cacttgtgacatC/Tggtagcatggag	Ile1324Ile	0.216
MPJ6_AC 2059*				Intron 28	**20352920**	IVS28 +172	agggaaggatagC/Tagccagggatca		0.004
MPJ6_AC 2060*				Intron 29	**20354201**	IVS29 +136	cttgagctagttC/Tcctaggatggac		0.002
MPJ6_AC 2061		**ssj0000408**	26	Intron 29	**20354219**	IVS29 +154	gatggacacgtcA/Gtttccagaactt		0.367
MPJ6_AC 2062		**IMS-JST090926**	17	Intron 29	**20355209**	IVS29 −35	cttttctggcatG/Aagcccaacagc		0.015
MPJ6_AC 2063*				Intron 30	**20358793**	IVS30 −92	gggggttttgaA/Gagtctgatctgg		0.008
MPJ6_AC 2064		**IMS-JST185750**		Intron 30	**20358832**	IVS30 −53	ccccctgcccctgC/Tgtctttccttgg		0.051
MPJ6_AC 2077*				3′-UTR	**20359975**	*61[c]	taattttatttttT/Gtataaaatacag		0.002
MPJ6_AC 2065*				3′-Flanking	**20360190**	*193+83[c]	ttattcctttgcC/Gtttcatttctgt		0.002a8

*Novel genetic variation

[a]delGCTTCCCAAACTTATTCGCAGTACTGGTGCCAGAATTTTGATAATACAAGAGCTTAGTAG/insTATTTACCT

[c]Numbered from the termination codon.

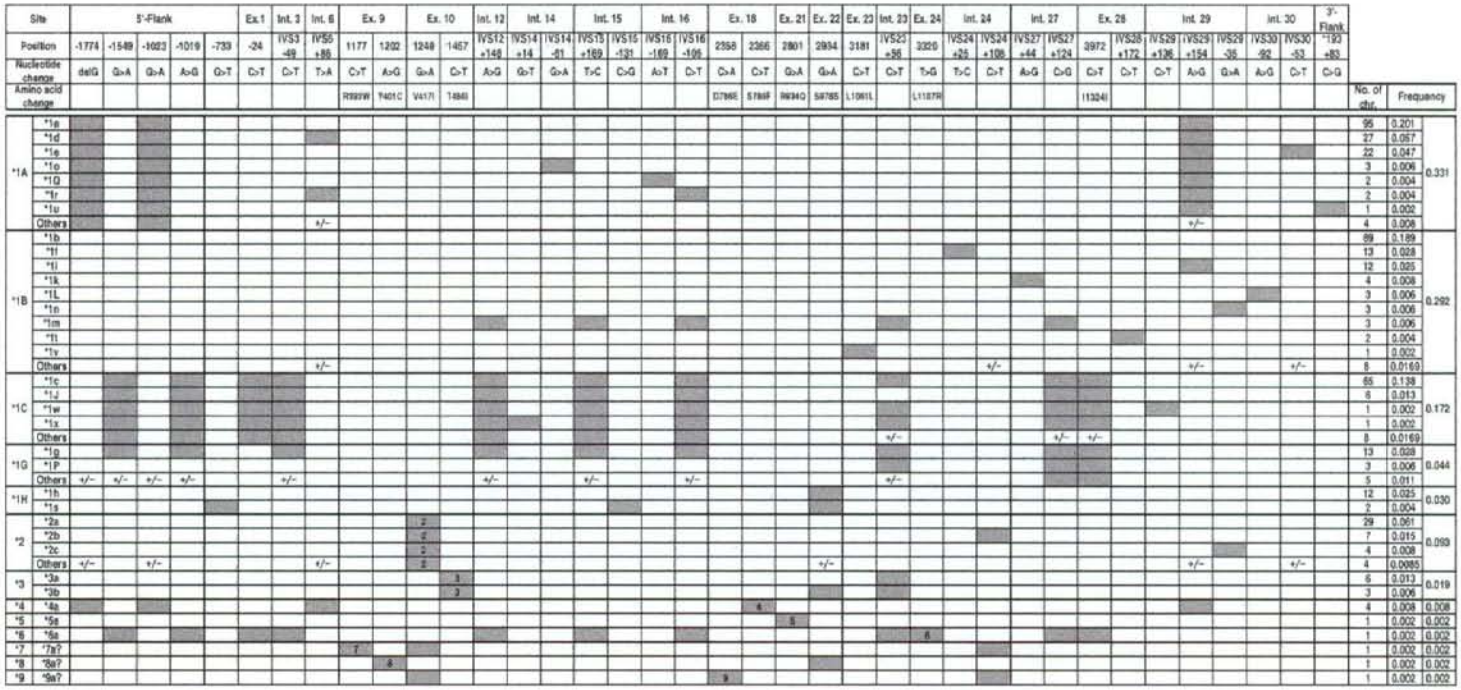

Fig. 2. *ABCC2* haplotypes in 236 Japanese subjects

The *1 groups (without nonsynonymous substitutions) were classified into *1A (harboring −1774delG), *1C (harboring −24C>T), *1G [harboring 3972C>T (Ile1324Ile) without −24C>T], *1H [harboring 2934G>A (Ser978Ser)] and *1B [without the common variations]. Marker SNPs for *2 to *9 are indicated by numbers. Rare and ambiguous haplotypes (n = 1) are shown with "?" or grouped into "others".

any amino acid substitution were assigned as the *1 group and named with small alphabetical letters in descending frequency order (*1a to *1x). Haplotypes with nonsynonymous variations were assigned from *2 to *9 groups, and their subtypes were named with small alphabetical letters. The haplotypes (*7a to *9a) were inferred in only one patient and described with "?" due to their ambiguity. Also, ambiguous rare haplotypes in the *1 and *2 groups were classified as "Others" in **Figure 2**. The *1 haplotypes were further classified into the *1A, *1B, *1C, *1G and *1H groups (capital alphabetical letters of the most frequent haplotypes were used) according to the common tagging SNPs, such as −1774delG, −24C>T, 3972C>T (Ile1324Ile), and 2937G>A (Ser978Ser).

The most frequent *1 group, *1A, harbors the common SNPs −1774delG and −1023G>A in the 5′-flanking region and mostly IVS29+154A>G, and the frequency of *1A (0.331) is almost the same as that in healthy Koreans (0.323) reported by Choi *et al.*[8] They have shown that −1774delG reduced promoter activity both at the basal level and after induction by chenodeoxycolic acid (CDCA), a component of bile acids, and that the haplotype bearing −1774delG is associated with chemical-induced hepatitis (cholestatis and mixed types).[8] Therefore, it is possible that *1A can affect the pharmacokinetics or pharmacodynamics of MRP2-transported drugs.

The *1B group haplotypes (0.292 frequency) harbor no or any intronic or synonymous variations the functions of which are unknown. The functional significance of variations in the *1B group, including the most frequent SNP IVS24+25T>C, needs further confirmation.

The third group *1C (0.172 frequency) harbors the known common SNPs −1549G>A, −1019A>G, −24C>T, IVS3−49C>T, and 3972C>T (Ile1324Ile), except for one rare ambiguous haplotype lacking 3972C>T (Ile1324Ile). The *1C haplotypes also harbor IVS12+148A>G, IVS15+169T>C and IVS16−105C>T. The haplotypes bearing −1549G>A, −24C>T and 3972C>T (Ile1324Ile) are commonly found in Korean populations (frequency 0.14–0.25)[8] and Caucasians (0.14–0.17).[10,14,21] The functional importance of the tagging SNP in the *1C group, −24C>T, has been reported by several researchers; *e.g.*, reduced promoter activity,[8,11] reduced mRNA expression in the kidney,[11] association with chemical-induced hepatitis (hepatocellular type),[8] and influence on irinotecan-pharmacokinetics and pharmacodynamics.[12,16] For other SNPs in the *1C group, functional alterations *in vitro* have not been shown; no change in promoter activity by −1549G>A, no influence of IVS3−49C>T on splicing, and no change induced by 3972C>T (Ile1324Ile) on MRP2 expression or transporter activity.[8] Although −24C>T caused reduced promoter activity in the absence of the bile acid CDCA,[8,11], enhanced promoter activity of −24C>T under induction by CDCA has been demonstrated.[8] Therefore the function of this SNP might depend on cholestatic status.

Our data demonstrated that −1019A>G was closely associated with the other *1C SNPs (complete linkage with −1549G>A). The close linkage between −1019A>G and −1549G>A was also observed in Caucasians, but their linkages with −24C>T and 3972C>T were relatively weak.[14] In contrast, another study on Caucasians reported that −1019A>G was exclusive to −1549G>A, −24C>T and 3972C>T.[10] Although the reasons for these discrepancies are not clear, some ethnic differences might exist in the 5′-flanking region.

The *1G group harbors 3972C>T (Ile1324Ile) but not −24C>T. Caucasians have haplotypes bearing 3972C>T (Ile1324Ile) without −24C>T at frequencies of 0.15–0.20.[10,21] In contrast, the frequency of the corresponding haplotype group in our study (*1G) was much lower (0.044). Although no *in vitro* effect of 3972C>T (Ile1324Ile) was shown,[8] its *in vivo* association with increased area under the concentration-time curve of irinotecan and its metabolites was reported in Caucasians.[13]

The *1H group (*1h and *1s) harbors a synonymous substitution of 2934G>A (Ser978Ser) (0.03 frequency). No influence of 2934G>A(Ser978Ser)on MRP2 expression or transport activity has been shown.[8]

As for haplotypes with nonsynonymous substitutions, eight haplotype groups (*2 to *9) were identified. The *2 [including 1249G>A (Val417Ile)] was the most frequent among them, and its frequency (0.093) was similar to those for Asians (0.10–0.13)[8,12,20] and slightly lower than those for Caucasians (0.13–0.22).[9,10,14,15,21] The haplotype frequencies of *3 [harboring 1457C>T (Thr486Ile)] and *4 [2366C>T (Ser789Phe)] were 0.019 and 0.008. Other rare haplotypes with novel nonsynonymous variation, *5 [2801G>A (Arg934Gln)], *6 [3320T>G (Leu1107Arg)], *7 [1177C>T (Arg393Trp)], *8 [1202A>G (Tyr401Cys)], and *9 [2358C>A (Asp786Glu)] were found each in only one subject as heterozygote at a 0.002 frequency. No functional significance of the marker SNP [1249G>A (Val417Ile)] of *2 has been shown *in vitro*,[8,23] but its *in vivo* associations with lower MRP2 expression in the placenta[24] and chemical-induced renal toxicity[25] have been reported. The variation 2366C>T (Ser789Phe) (*4) has been shown to cause reduced MRP2 expression and alter localization *in vitro*,[23] but clinical data are limited. Functional changes in *3 [1457C>T (Thr486Ile)] and *5 to *9 (novel nonsynonymous variations) are currently unknown. Possible effects of these amino acid substitutions were speculated using PolyPhen analysis (http://genetics.bwh.harvard.edu/pph); its prediction is based on the analysis of substitution site [e.g., a substitution in transmenbrane domain is assessed by the predicted hydrophobic and transmembrane (PHAT) matrix score], likelihood of the substitution assessed by the position-specific independent count (PSIC) profile scores, and protein 3D structures. This analysis predicted a possible functional change of Leu1107Arg (*6) due to substitution in

the transmembrane region (PHAT matrix element difference = −6), and probable functional effects of Arg393Trp (*7) (PSIC score difference = 3.053), Tyr401Cys (*8) (3.382) and Asp786Glu (*9) (2.277), but no functional effects of *3 (1.446) and *5 (0.326).

In conclusion, the current study provided detailed information on *ABCC2* variations and haplotype structures in Japanese and also suggested a large ethnic difference in the frequencies of 3972C>T(Ile1324Ile) and 1446C>G (Thr482Thr) and their related haplotypes between Asians and Caucasians. This information would be useful for studies investigating the clinical significance of *ABCC2* alleles and haplotypes.

Acknowledgements: The authors thank Ms. Chie Sudo for her secretarial assistance.

References

1) Jedlitschky, G., Hoffmann, U. and Kroemer, H. K.: Structure and function of the MRP2 (ABCC2) protein and its role in drug disposition. *Expert Opin. Drug Metab. Toxicol.*, **2**: 351–66 (2006).
2) Wada, M.: Single nucleotide polymorphisms in *ABCC2* and *ABCB1* genes and their clinical impact in physiology and drug response. *Cancer Lett.*, **234**: 40–50 (2006).
3) Huang, Y.: Pharmacogenetics/genomics of membrane transporters in cancer chemotherapy. *Cancer Metastasis Rev.*, **26**: 183–201 (2007).
4) Taniguchi, K., Wada, M., Kohno, K., Nakamura, T., Kawabe, T., Kawakami, M., Kagotani, K., Okumura, K., Akiyama, S. and Kuwano, M.: A human canalicular multispecific organic anion transporter (cMOAT) gene is overexpressed in cisplatin-resistant human cancer cell lines with decreased drug accumulation. *Cancer Res.*, **56**: 4124–4129 (1996).
5) Hinoshita, E., Uchiumi, T., Taguchi, K., Kinukawa, N., Tsuneyoshi, M., Maehara, Y., Sugimachi, K. and Kuwano, M.: Increased expression of an ATP-binding cassette superfamily transporter, multidrug resistance protein 2, in human colorectal carcinomas. *Clin. Cancer Res.*, **6**: 2401–2407 (2000).
6) Cui, Y., Konig, J., Buchholz, J.K., Spring, H., Leier, I. and Keppler, D.: Drug resistance and ATP-dependent conjugate transport mediated by the apical multidrug resistance protein, MRP2, permanently expressed in human and canine cells. *Mol. Pharmacol.*, **55**: 929–937 (1999).
7) Wada, M., Toh, S., Taniguchi, K., Nakamura, T., Uchiumi, T., Kohno, K., Yoshida, I., Kimura, A., Sakisaka, S., Adachi, Y. and Kuwano, M.: Mutations in the canilicular multispecific organic anion transporter (cMOAT) gene, a novel ABC transporter, in patients with hyperbilirubinemia II/Dubin-Johnson syndrome. *Hum. Mol. Genet.*, **7**: 203–207 (1998).
8) Choi, J. H., Ahn, B. M., Yi, J., Lee, J. H., Lee, J. H., Nam, S. W., Chon, C. Y., Han, K. H., Ahn, S. H., Jang, I. J., Cho, J. Y., Suh, Y., Cho, M. O., Lee, J. E., Kim, K. H. and Lee, M. G..: MRP2 haplotypes confer differential susceptibility to toxic liver injury. *Pharmacogenet. Genomics*, **17**: 403–415 (2007).
9) Daly, A. K., Aithal, G. P., Leathart, J. B., Swainsbury, R. A., Dang, T. S. and Day, C. P.: Genetic susceptibility to diclofenac-induced hepatotoxicity: contribution of UGT2B7, CYP2C8, and ABCC2 genotypes. *Gastroenterology*, **132**: 272–281 (2007).
10) de Jong, F. A., Scott-Horton, T. J., Kroetz, D. L., McLeod, H. L., Friberg, L. E., Mathijssen, R. H., Verweij, J., Marsh, S. and Sparreboom, A.: Irinotecan-induced diarrhea: functional significance of the polymorphic ABCC2 transporter protein. *Clin. Pharmacol.Ther.*, **81**: 42–49 (2007).
11) Haenisch, S., Zimmermann, U., Dazert, E., Wruck, C. J., Dazert, P., Siegmund, S., Kroemer, H. K., Warzok, R. W. and Cascorbi, I.: Influence of polymorphisms of ABCB1 and ABCC2 on mRNA and protein expression in normal and cancerous kidney cortex. *Pharmacogenomics J.*, **7**: 56–65 (2007).
12) Han, J. Y., Lim, H. S., Yoo, Y. K., Shin, E. S., Park, Y. H., Lee, S. Y., Lee, J. E., Lee, D. H., Kim, H. T. and Lee, J. S.: Associations of ABCB1, ABCC2, and ABCG2 polymorphisms with irinotecan-pharmacokinetics and clinical outcome in patients with advanced non-small cell lung cancer. *Cancer*, **110**: 138–147 (2007).
13) Innocenti, F., Undevia, S. D., Chen, P. X., Das, S., Ramirez, J., Dolan, M. E., Relling, M. V., Kroetz, D. L. and Ratain, M. J.: Pharmacogenetic analysis of interindividual irinotecan (CPT-11) pharmacokinetic (PK) variability: Evidence for a functional variant of ABCC2. *2004 ASCO Annual Meeting Proceedings (Post-Meeting Edition)*. Vol. 22, No. 14S (July 15 Supplement), 2004: Abstract No: 2010.
14) Naesens, M., Kuypers, D. R., Verbeke, K. and Vanrenterghem, Y.: Multidrug resistance protein 2 genetic polymorphisms influence mycophenolic acid exposure in renal allograft recipients. *Transplantation*, **82**: 1074–1084 (2006).
15) Rau, T., Erney, B., Gores, R., Eschenhagen, T., Beck, J. and Langer, T.: High-dose methotrexate in pediatric acute lymphoblastic leukemia: impact of ABCC2 polymorphisms on plasma concentrations. *Clin. Pharmacol. Ther.*, **80**: 468–476 (2006).
16) Zhou, Q., Sparreboom, A., Tan, E. H., Cheung, Y. B., Lee, A., Poon, D., Lee, E. J. and Chowbay, B.: Pharmacogenetic profiling across the irinotecan pathway in Asian patients with cancer. *Br. J. Clin. Pharmacol.*, **59**: 415–424 (2005).
17) Niemi, M, Arnold, K. A., Backman, J. T., Pasanen, M. K., Godtel-Armbrust, U., Wojnowski, L., Zanger, U. M., Neuvonen, P. J., Eichelbaum, M., Kivisto, K. T. and Lang, T.: Association of genetic polymorphism in ABCC2 with hepatic multidrug resistance-associated protein 2 expression and pravastatin pharmacokinetics. *Pharmacogenet. Genomics.*, **16**: 801–808 (2006).
18) Itoda, M., Saito, Y., Soyama, A., Saeki, M., Murayama, N., Ishida, S., Sai, K., Nagano, M., Suzuki, H., Sugiyama, Y., Ozawa, S. and Sawada, J.: Polymorphisms in the *ABCC2* (cMOAT/MRP2) gene found in 72 established cell lines derived from Japanese individuals: an association between single nucleotide polymorphisms in the 5′-untranslated region and exon 28. *Drug Metab. Dispos.*, **30**: 363–364 (2002).
19) Kitamura, Y., Moriguchi, M., Kaneko, H., Morisaki, H., Morisaki, T., Toyama, K. and Kamatani, N.: Determination of probability distribution of diplotype configuration (diplotype distribution) for each subject from genotypic data using the EM algorithm. *Ann. Hum. Genet.*, **66**: 183–193 (2002).
20) Ito, S., Ieiri, I., Tanabe, M., Suzuki, A., Higuchi, S. and Otsubo, K.: Polymorphism of the ABC transporter genes, MDR1, MRP1 and MRP2/cMOAT, in healthy Japanese subjects. *Pharmacogenetics*, **11**: 175–184 (2001).
21) Bosch, T. M., Doodeman, V. D., Smits, P. H., Meijerman, I., Schellens, J. H. and Beijnen, J. H.: Pharmacogenetic screening

for polymorphisms in drug-metabolizing enzymes and drug transporters in a Dutch population. *Mol. Diagn. Ther.*, **10**: 175–185 (2006).

22) Nebert, D. W.: Suggestions for the nomenclature of human alleles: relevance to ecogenetics, pharmacogenetics and molecular epidemiology. *Pharmacogenetics*, **10**: 279–290 (2000).

23) Hirouchi, M., Suzuki, H., Itoda, M., Ozawa, S., Sawada, J., Ieiri, I., Ohtsubo, K. and Sugiyama, Y.: Characterization of the cellular localization, expression level, and function of SNP variants of MRP2/ABCC2. *Pharm. Res.*, **21**: 742–748 (2004).

24) Meyer zu Schwabedissen, H. E., Jedlitschky, G., Gratz, M., Haenisch, S., Linnemann, K., Fusch, C., Cascorbi, I. and Kroemer, H. K.: Variable expression of MRP2 (ABCC2) in human placenta: influence of gestational age and cellular differentiation. *Drug Metab. Dispos.*, **33**: 896–904 (2005).

25) Izzedine, H., Hulot, J. S., Villard, E., Goyenvalle, C., Dominguez, S., Ghosn, J., Valantin, M. A., Lechat, P. and Deray, A. G.: Association between *ABCC2* gene haplotypes and tenofovir-induced proximal tubulopathy. *J. Infect. Dis.*, **194**: 1481–1491 (2006).

26) Saito, S., Iida, A., Sekine, A., Miura, Y., Ogawa, C., Kawauchi, S., Higuchi, S. and Nakamura, Y.: Identification of 779 genetic variations in eight genes encoding members of the ATP-binding cassette, subfamily C (ABCC/MRP/CFTR. *J. Hum. Genet.*, **47**: 147–171 (2002).

Available online at www.sciencedirect.com
ScienceDirect
Journal of Controlled Release 125 (2008) 137–144
journal of controlled release
www.elsevier.com/locate/jconrel

Tumor specific ultrasound enhanced gene transfer *in vivo* with novel liposomal bubbles

Ryo Suzuki [a], Tomoko Takizawa [a], Yoichi Negishi [b], Naoki Utoguchi [a], Kaori Sawamura [a], Kumiko Tanaka [a], Eisuke Namai [a], Yusuke Oda [a], Yasuhiro Matsumura [c], Kazuo Maruyama [a,*]

[a] *Department of Biopharmaceutics, School of Pharmaceutical Sciences, Teikyo University, 1091-1 Suwarashi, Sagamiko, Sagamihara, Kanagawa 229-0195, Japan*
[b] *Department of Drug and Gene Delivery System, School of Pharmacy, Tokyo University of Pharmacy and Life Science, Hachioji, Tokyo, Japan*
[c] *Investigative Treatment Division, Research Center for Innovative Oncology, National Cancer Center Hospital East, Kashiwa, Chiba, Japan*

Received 30 November 2006; accepted 19 August 2007
Available online 29 August 2007

Abstract

Bubble liposomes (liposomes which entrap an ultrasound imaging gas) may constitute a unique system for delivering various molecules efficiently into mammalian cells *in vitro*. In this study, Bubble liposomes were compared with cationic lipid (CL)–DNA complexes as potential gene delivery carriers into tumor *in vivo*. The delivery of genes by Bubble liposomes depended on the intensity of the applied ultrasound. Transfection efficiency plateaued at 0.7 W/cm^2 ultrasound intensity. Bubble liposomes efficiently transferred genes into cultured cells even when the cells were exposed to ultrasound for only 1 s. In addition, Bubble liposomes could introduce the luciferase gene more effectively than CL-DNA complexes into mouse ascites tumor cells and solid tumor tissue. We conclude that the combination of Bubble liposomes and ultrasound is a minimally-invasive and tumor specific gene transfer method *in vivo*.

Keywords: Liposomes; Bubble liposomes; Gene delivery; Ultrasound; Cancer

1. Introduction

In cancer gene therapy, it is important to develop the easy, safe, efficient, minimally-invasive and tissue-specific technologies of gene transfer into tumor tissue. Sonoporation is a method of gene delivery with ultrasound. Ultrasound increases the permeability of the plasma membrane and reduces the thickness of the unstirred layer of the cell surface, aiding DNA entry into cells [1,2]. Preliminary studies into the utility of ultrasound for gene delivery used frequencies in the range of 20–50 kHz [1,3]. However, these frequencies are also known to induce tissue damage and cavitation if not properly controlled [4–6]. To overcome this problem, several studies have used frequencies of 1–3 MHz, intensities of 0.5–2 W/cm^2, and pulse-modulation [7–9]. In a separate approach, a combination of therapeutic ultrasound and microbubble echo contrast agents was shown to enhance gene transfection efficiency [10–15] by effectively and directly transferring DNA into the cytosol. Microbubbles based on protein microspheres, and sugar microbubbles, are commercially available; however, although they encapsulate ultrasound contrast agents, they are too large (2–10 μm diameter) for intravascular application [16]. It has been reported that the *i.v.* injection of Optison without ultrasound exposure results in lethal embolisms in vital organs in mice [17]. Although a similar effect has not been observed in humans, it is possible that Optison can not pass through capillary vessels. Ideally, microbubbles should be smaller than red blood cells.

Liposomes can be used as drug, antigen and gene delivery carriers [18–26]. Based on liposome technology, we developed novel liposomal bubbles (Bubble liposomes) containing the ultrasound imaging gas, perfluoropropane. When coupled with ultrasound exposure, Bubble liposomes can be used as novel

* Corresponding author. Tel.: +81 42 685 3722; fax: +81 42 685 3432.
E-mail address: maruyama@pharm.teikyo-u.ac.jp (K. Maruyama).

0168-3659/$ - see front matter © 2007 Elsevier B.V. All rights reserved.
doi:10.1016/j.jconrel.2007.08.025

gene delivery agents [27]. In addition, we found out that the gene delivery was only observed at the site of ultrasound exposure. Therefore, using Bubble liposomes and ultrasound, we could establish minimally-invasive and tumor tissue-specific gene delivery. In the present study, the characteristics of Bubble liposomes as gene delivery vectors were studied, and gene transfection efficiencies into tumor *in vivo* were compared with lipofection using cationic liposomes, a common non-viral gene transfer method.

2. Materials and methods

2.1. Cells

African green monkey kidney fibroblast COS-7 cells were cultured in Dulbecco's modified Eagle's medium (DMEM; Sigma Chemical Co., St. Louis, MO) supplemented with 10% heat inactivated fetal Bovine serum (FBS, GIBCO, Invitrogen Co., Carlsbad, CA). Mouse Sarcoma-180 (S-180) cells were cultured in Eagle's medium (MEM; Sigma) supplemented with 10% heat inactivated FBS. All culture media contained 100 U/mL penicillin (Wako Pure Chemical Industries, Ltd., Osaka, Japan) and 100 μg/mL streptomycin (Wako).

2.2. Preparation of liposomes and Bubble liposomes

Liposomes composed of 1,2-distearoyl-sn-glycero-phosphatidylcholine (DSPC) (NOF Corporation, Tokyo, Japan) and 1,2-distearoyl-sn-glycero-3-phosphatidyl-ethanolamine-methoxy-polyethyleneglycol (DSPE-PEG (2 k)–OMe; NOF) (94:6 (m/m)) were prepared by reverse phase evaporation. In brief, all reagents (total lipid: 100 μmol) were dissolved in 8 mL of 1:1 (v/v) chloroform/diisopropyl ether, then 4 mL of PBS was added. The mixture was sonicated and evaporated at 65 °C. The solvent was completely removed, and the size of the liposomes was adjusted to less than 200 nm using an extruding apparatus (Northern Lipids Inc., Vancouver, BC) and sizing filters (pore sizes: 100 nm and 200 nm; Nuclepore Track-Etch Membrane, Whatman plc, UK). After sizing, the liposomes were sterilized by passing them through a 0.45 μm pore size filter (MILLEX HV filter unit, Durapore PVDF membrane, Millipore Corporation, MA). The liposome size was measured with dynamic light scattering (ELS-800, Otsuka Electronics Co., Ltd., Osaka, Japan). The average diameter of these liposomes were about 150–200 nm. Lipid concentration was measured with the Phospholipid C test wako (Wako Pure Chemical Industries). Bubble liposomes were prepared from the liposomes and perfluoropropane gas (Takachiho Chemical Ind. Co. Ltd., Tokyo, Japan). In brief, 5 mL sterilized vials containing 2 mL of the liposome suspension (lipid concentration: 1 mg/mL) were filled with perfluoropropane, capped and then supercharged with 7.5 mL of perfluoropropane. The vial was placed in a bath-type sonicator (42 kHz, 100 W; BRANSONIC 2510J-DTH, Branson Ultrasonics Co., Danbury, CT) under the condition of positive pressure with perfuluoropropane in the vial under the condition of positive pressure with perfuluoropropane in the vial for 5 min to form the Bubble liposomes.

2.3. Microscopic observation of Optison and Bubble liposomes and size distribution

Optison (NEPA GENE, CO., LTD., Chiba, Japan) or Bubble liposomes were placed on glass slides, covered with a cover slip and observed with a microscope (Leica MICROSYSTEMS, Wetzlar, Germany) using a darklite illuminator (NEPA GENE). The size distribution of Optison and Bubble liposomes was measured by dynamic light scattering (ELS-800).

2.4. Transmission electron microscopy of Bubble liposomes

Bubble liposomes were suspended into sodium alginate solution (0.2% (w/v) in PBS). This suspension was dropped into calcium chloride solution (100 mM) to hold Bubble liposomes within calcium alginate gel. Then, the beads of calcium alginate gel containing Bubble liposomes were prefixed with 2% glutaraldehyde solution in 0.1 M Cacodylate buffer, post-fixed with 2% OsO_4, dehydrated with an ethanol series, and then embedded in Epan812 (polymerized at 60 °C). Ultrathin sections were made with an ultramicrotome at a thickness of 60–80 nm. Ultrathin sections were mounted on 200 mesh copper grids. They were stained with 2% uranyl acetate for 5 min and Pb for 5 min. The samples were observed with JEOL JEM12000EX at 100 kV. The treatment after prefixation was carried out in Hanaichi Ultrastructure Research Institute Co.,Ltd (Aichi, Japan).

2.5. Transfection of plasmid DNA into cells using Bubble liposomes

Luciferase cording plasmid DNA (pCMV-Luc), COS-7 cells (1×10^5 cells) and Bubble liposomes (60 μg) were suspended in culture medium (500 μL) with 10% FBS in 2 mL polypropylene tubes. The suspension was ultrasonicated using a Sonopore 4000 (6 mm diameter probe; NEPA GENE) sonicator under various conditions. The cells were washed twice with PBS, resuspended in fresh culture medium and cultured in 48-well plates for 2 days.

2.6. Transfection of plasmid DNA into cells by lipofection

Plasmid DNA (pCMV-Luc, 0.25 μg) and Lipofectin (1.25 μg) (Invitrogen) were mixed and complexed according to the manufacturer's instructions. The complex was added to COS-7 cell suspensions (1×10^5 cells/500 μL/ tube) containing various concentrations of serum for 10 s. The cells were washed twice with PBS, resuspended in fresh culture medium and cultured in 48-well plates for 2 days.

2.7. In vivo gene delivery into mouse ascites tumor cells

S-180 cells (1×10^6 cells) were *i.p.* injected into ddY mice (4 weeks old, male) (Sankyo Labo Service Corporation, Tokyo, Japan) on day 0. When S-180 cells grew as the ascites tumor in mice after 8 days of the injection [28], the mice were anaesthetized with NEMBUTAL (50 mg/kg) (Dainippon

Sumitomo Pharma, Osaka, Japan), then injected with 510 μL of pCMV-Luc (10 μg) and Bubble liposomes (500 μg) in PBS. Ultrasound (frequency: 1 MHz, duty: 50%; intensity: 1.0 W/cm^2, time: 1 min) was transdermally applied to the abdominal area using a Sonopore 3000 ultrasonicator with a probe of diameter 20mm (NEPA GENE). In other experiments, pCMV-Luc (10μg) and Lipofectin (50μg) or Lipofectamine 2000 (50μg) were mixed and complexed according to the manufacturer's instructions. The complex was suspended in PBS (510μL) and injected into the peritoneal cavities of mice. After 2days, S-180 cells were recovered from the abdomens of the mice. Then, the recovered cells were lysed in the lysis buffer (0.1M Tris–HCl (pH 7.8), 0.1% Triton X-100, 2mM EDTA) and luciferase activity was determined.

2.8. In vivo gene delivery into mouse footpad solid tumor

S-180 cells (1×10^6 cells) were inoculated into the left footpad of ddY mice (5 weeks old, male). At day 4, when the thickness of the footpad was over 3.5 mm (normal thickness was about 2 mm), the left femoral artery was exposed. One hundred μL of pCMV-Luc (10 μg) with or without Bubble liposomes (100 μg) were injected into femoral artery using 30-gauge needle. In the same time, ultrasound (frequency: 0.7 MHz, duty: 50%; intensity: 1.2 W/cm^2, time: 2 min) was transdermally applied to the tumor tissue using a Sonopore 4000 ultrasonicator with a probe of diameter 8 mm (NEPAGENE). The needle hole was then closed with an adhesive agent (Aron Alpha; Sankyo, Tokyo, Japan) and skin was put in a suture. In other samples, pCMV-Luc (10 μg) and Lipofectamine 2000 (25 μg) (Invitrogen Corporation, Carlsbad, CA) were mixed and complexed according to manual of Lipofectamine 2000. The complex were suspended in PBS (100 μL) and injected into femoral artery of mice. After 2 days of injection, the mice were sacrificed and the tumor tissues were collected. Then, the tumor tissues were homogenated in the lysis buffer and luciferase activity was determined.

2.9. Luciferase assay

Luciferase activity was measured using a luciferase assay system (Promega, Madison, WI) and a luminometer (TD-20/20, Turner Designs, Sunnyvale, CA). Activity is reported in relative light units (RLU) per mg protein.

2.10. In vivo Luciferase imaging

The mice were anaesthetized and *i.p.* injected with D-luciferin (150 mg/kg) (Xenogen, Corporation, CA). After 10 min, luciferase expression was observed with *in vivo* luciferase imaging system (IVIS) (Xenogen Corporation).

2.11. Hemolysis assay

Mouse red blood cells (2.5×10^8 cells/500 μL) were exposed with ultrasound (frequency: 0.7 MHz, Duty: 50%, Intensity: 0.5–1.5 W/cm^2, Time: 10 s.) in absent or present of Bubble liposomes. The red blood cell suspension was centrifuged for 10 min at 3000 rpm. Then, absorbance ($A_{540\ nm}$) of the supernatant was measured. The rate of hemolysis was calculated as follows: % of hemolysis=($A_{540\ nm}$ of experimental group $-A_{540\ nm}$ of non-treated group)/($A_{540\ nm}$ of hypotonic solution treated group $-A_{540\ nm}$ of non-treated group)$\times$100.

2.12. In vivo studies

All experimental protocols for animal studies were in accordance with the Principle of Laboratory Animal Care in Teikyo University.

2.13. Statistical analysis

Differences in luciferase activity between experimental groups were compared with non-repeated measures ANOVA and Dunnett's test.

3. Results and discussion

The use of non-viral vectors is attractive as a safe, clinically acceptable gene therapy technique. In addition, non-viral vectors should be easy to prepare and use. However, most non-viral vectors deliver plasmid DNA into cells via endocytosis, followed by plasmid DNA degradation in the endosomes. Consequently, non-viral vectors often result in low gene delivery efficiency. It has been reported that new types of non-viral vectors can induce the escape of genes from endosomes [29–31] and directly deliver genes into the cytosol via a fusion mechanism [28,32]. In addition, microbubbles and ultrasound have been investigated with a view to improving the transfection efficiency of non-viral vectors. Gene delivery using a combination of microbubbles such as Optison and ultrasound has been widely reported. In order for extracellular plasmid DNA to be directly and effectively delivered into the cytosol, transient pores in the cell membrane must be formed by cavitation. However, conventional microbubbles are very large, with most greater than 2 μm in diameter [16]. Actually, our observations of Optison using a microscope and a darklite illuminator showed some bubbles more than 10 μm in diameter (Fig. 1(a)). In the measurement of the size distribution, there were some large microbubbles (Fig. 1d)). Tsunoda et al. pointed out that these large bubbles might cause lethal embolism in some vital organs [17]. In contrast, most Bubble liposomes were much smaller than Optison, with average diameters less than 2 μm (Fig. 1(b, e)). The injection of 1 mg of Bubble liposomes into the tail veins of mice was not lethal (data not shown), suggesting that Bubble liposomes may not cause lethal embolism. To confirm the structure of Bubble liposomes, we observed Bubble liposome with transmission electron microscopy (Fig. 1(c)). Interestingly, there were nanobubbles into lipid bilayer. From this result, it was thought that Bubble liposomes were different from conventional microbubbles which was the echo gas wrapped with lipid mono-layer. Kodama T. et al. and Klibanov A.L. et al. reported about microbubbles using distearoylphospatidylcholine and PEG-

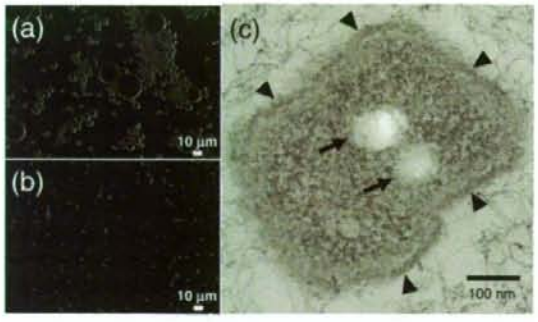

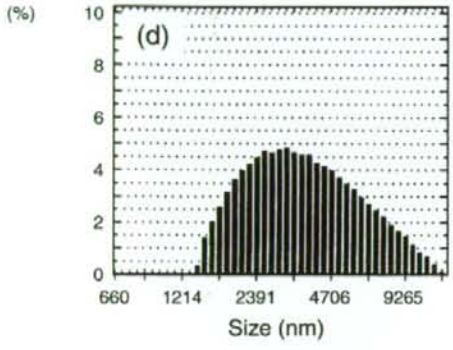

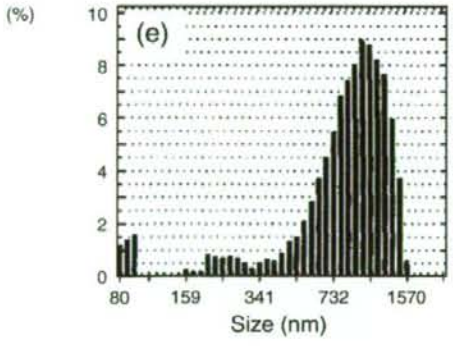

Fig. 1. Microscopy of Optison and Bubble liposomes. Optison (a) and Bubble liposomes (b) were observed with a microscope using a darklite illuminator. Original magnification ×400. Bubble liposomes (c) were observed with a transmission electric microscope at 100 kV. Original magnification ×50,000. Arrow head shows lipid bi-layer and arrow shows perfluoropropane nanobubble. The size distribution of Optison (d) and Bubble liposomes (e).

stearate [33,34]. These microbubbles were made by being stabilized hydrophobic echo gas with amphipathic molecules such as lipid and surfactant. In our method, it was thought that liposomes were reconstituted by sonication under the condition of supercharge with perfluoropropane in the 5 mL vial container. At the same time, perfluoropropane would be entrapped within lipids like micelles, which were made by DSPC and DSPE-PEG (2 k)-OMe from liposome composition, to form nanobubbles. The lipid nanobubbles were encapsulated within the reconstituted liposomes (Fig. 1(c)), which sizes were changed into around 1 μm (Fig. 1(b,e)) from 150–200 nm of original. In addition, we evaluated about the stability of Bubble liposomes by transfection efficiency with sonoporation (Fig. 2). The efficiency gradually decreased according to storage time. We also observed the aspect and ultrasound imaging of Bubble liposomes. The suspension of Bubble liposomes gradually became clear in aspects, resulted in decreasing the echo signal according to storage time (data not shown). These results suggested that perfluoropropane was gradually degassed from Bubble liposomes. Therefore, we used fresh Bubble liposomes in all experiments.

Previously, we reported that Bubble liposomes could induce cavitation and deliver plasmid DNA into various types of cells [27]. In order to examine what conditions are necessary for Bubble liposomes to efficiently deliver genes, transfection efficiency was assessed using Bubble liposomes combined with various levels of ultrasound exposure (Fig. 3(a)). COS-7 cells were exposed to various intensities of ultrasound in the presence of Bubble liposomes for 10 s. Gene transfection efficiency increased with increasing ultrasound intensity and reached a plateau at 0.7 W/cm^2. No cytotoxicity was evident even at 2.5 W/cm^2 (data not shown). The length of ultrasound exposure required to achieve gene expression was examined by measuring gene expression after 0, 1, 5 and 10 s of exposure (Fig. 3(b)). Surprisingly, gene expression was observed after 1 s of ultrasound exposure in the presence of Bubble liposomes. Transfection efficiency depended on ultrasound exposure time and reached a plateau after 5 s exposure. Efficiency was found to depend on both ultrasound intensity and exposure time (Fig. 3), indicating that Bubble liposomes can rapidly induce gene delivery while requiring only weak ultrasound, and without inducing cytotoxicity. Five seconds or 0.7 W/cm^2 of ultrasound exposure resulted in maximal gene expression, presumably due to bubble cavitation.

The transfection efficiency of some cationic non-viral vectors is significantly decreased in the presence of serum

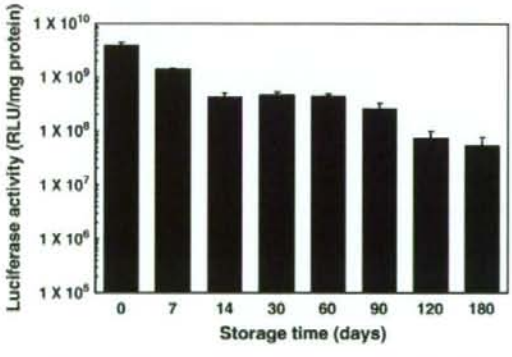

Fig. 2. Stability of Bubble liposomes. After preparation of Bubble liposomes, the vial containing Bubble liposomes was put in the refrigerator for each period. After storage, the transfection efficiency was measured with each samples. COS-7 cells (1×10^5 cells/500 μL) were mixed with pCMV-Luc (5 μg) and Bubble liposomes (60 μg). The cell mixture was exposed to ultrasound (frequency: 2 MHz, duty: 50%, burst rate: 2 Hz, intensity: 2.5 W/cm^2, time: 10 s.). The cells were washed and cultured for 2 days, then luciferase activity was determined as described in Materials and methods. Each bar represents the mean ± S.D. for triplicate.

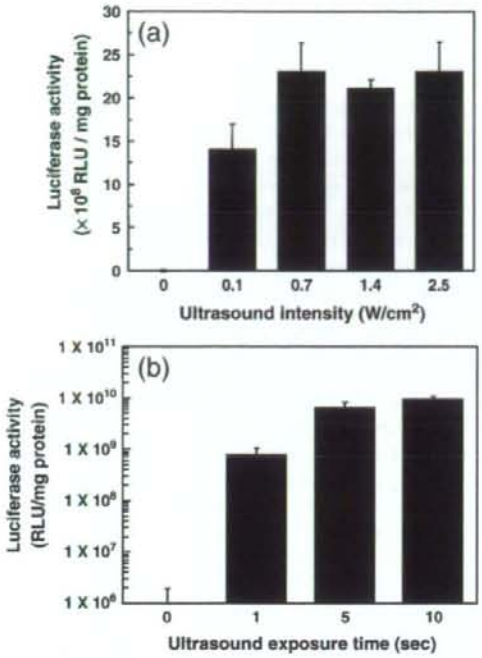

Fig. 3. Effect of ultrasound conditions on transfection efficiency with Bubble liposomes. COS-7 cells (1×10^5 cells/500 μL) were mixed with pCMV-Luc (5 μg) and Bubble liposomes (60 μg). The cell mixture was exposed to ultrasound (a): (frequency: 2 MHz, duty: 50%, burst rate: 2 Hz, intensity: 0–2.5 W/cm^2, time: 10 s.) or (b): (frequency: 2 MHz, duty: 50%, burst rate: 2 Hz, intensity: 2.5 W/cm^2, time: 0–10 s.). The cells were washed and cultured for 2 days, then luciferase activity was determined as described in Materials and methods. Each bar represents the mean±S.D. for triplicate.

due to an interaction between serum proteins and the cationic vectors [28]. Whereas, transfection efficiency with the combination of Bubble liposomes and ultrasound did not decrease even in the presence of 50% serum in *in vitro* study [27]. In the next examination, we examined whether Bubble liposomes could deliver plasmid DNA into S-180 ascites tumor cells in living animals after local injection (Fig. 4). In this examination, we compared the transfection efficiency with Bubble liposomes or cationic liposomes such as Lipofectin and Lipofectamine 2000. Luciferase expression was low in the mice treated with lipofectin-plasmid DNA complexes prepared by the traditional lipofection method, presumably because the complexes were associated with various proteins in the peritoneal cavity. On the other hand, luciferase expression increased in the mice treated with Lipofectamine 2000-plasmid DNA complexes compare with Lipofectin, because it was known that LF2000 was better than Lipofectin for gene delivery in the presence of serum. In addition, luciferase expression in mice treated with plasmid DNA, Bubble liposomes and ultrasound exposure was higher than that in the mice treated with Lipofectamine 2000-plasmid DNA complexes. This result supported the previous our report. In short, it was thought that Bubble liposomes and ultrasound was not affected by proteins existing in the peritoneal cavity and this method immediately and directly delivered plasmid DNA into cells with the mechanism which was not endocytosis pathway in lipofection method. We also confirmed that ultrasound combined with Bubble liposomes was effective at delivering genes to other tissues in the peritoneal cavity such as stomach, kidney, liver, spleen, intestine, diaphragm, pancreas, peritoneum and mesentery. Luciferase activity in these tissues was much lower than that observed in the S-180 cells (less than 130 RLU/mg protein).

Mizuguchi et al. reported about the effective cancer gene therapy by cytokine provision in the local area via gene delivery into arteries leading to tumor or arteries in tumor tissue [35]. Previously, we succeeded the gene delivery into artery of ultrasound exposure site with Bubble liposomes [27]. Therefore, we thought that our technology could be applied to establish the tumor tissue specific gene delivery. In this time, we attempted to deliver plasmid DNA to solid tumor via the injection into the artery that lead to tumor (Fig. 5). In Fig. 4, Lipofectin did not work well as gene delivery tool. In this study, we only used Lipofectamine 2000 as a control. In the mice treated with plasmid DNA and ultrasound, luciferase expression was same low level in the mice of plasmid DNA injection. And, luciferase expression was also low level in the mice treated with Lipofectamine 2000 and plasmid DNA complex, although the complex could be induced into S-180 ascites tumor cells. Generally, enough time is necessary for the complex to bind to cell surface and deliver plasmid DNA into cells. In this case, there was no time for the complex to retain in tumor tissue after injection because of blood stream and it would be resulted in

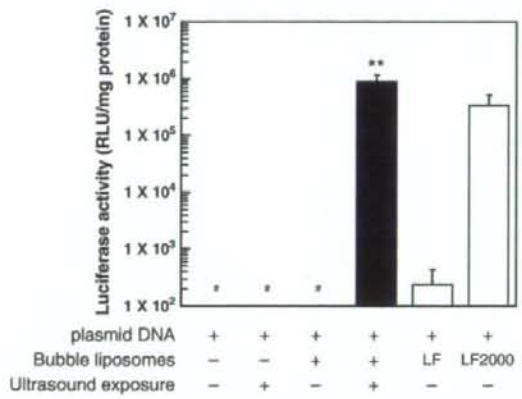

Fig. 4. *In vivo* gene delivery into mouse ascites tumor cells with Bubble liposomes. S-180 cells (1×10^6 cells) were i.p. injected into ddY mice. After 8 days, the mice were anaesthetized, then injected with 510 μL of pCMV-Luc (10 μg) and Bubble liposomes (500 μg) in PBS. Ultrasound (frequency: 1 MHz, duty: 50%; intensity: 1.0 W/cm^2, time: 1 min) was transdermally applied to the abdominal area. In another experiment, pCMV-Luc (10 μg) — Lipofectin (50 μg) or Lipofectamine 2000 (50 μg) complex was suspended in PBS (510 μL) and injected into the peritoneal cavity of mice. After 2 days, S-180 cells were recovered from the abdomens of the mice. Luciferase activity was determined as described in Materials and methods. Each bar represents the mean±S.D. for three to six mice/group. $^{**}P<0.01$ compared to the group treated with plasmid DNA, Bubble liposomes, ultrasound exposure or lipofection with Lipofectin or Lipofectamine 2000. LF, Lipofectin. LF2000, Lipofectamine 2000. #$<10^2$ RLU/mg protein.

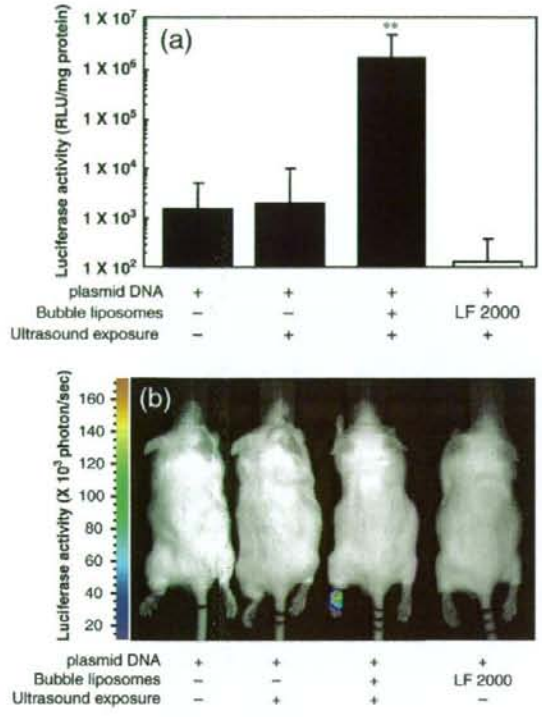

Fig. 5. *In vivo* gene delivery into mouse solid tumor with Bubble liposomes. S-180 cells (1×10^6 cells) were inoculated into left footpad of ddY mice. After 4 days, the mice were anaesthetized, then injected with 100 mL of pCMV-Luc (10 μg) in absent or present of Bubble liposomes (100 μg) in PBS. Ultrasound (frequency: 0.7 MHz, duty: 50%; intensity: 1.2 W/cm^2, time: 1 min) was transdermally exposed to tumor tissue. In another experiment, pCMV-Luc (10 μg) — Lipofectamine 2000 (25 μg) complex was suspended in PBS (100 μL) and injected into the left femoral artery. After 2 days, tumor tissue was recovered the mice. Luciferase activity was determined as described in Materials and methods. (a) Luciferase activity in solid tumor. Each bar represents the mean ± S.D. for five mice/group. $^{**}P<0.01$ compared to the group treated with plasmid DNA, ultrasound exposure or Lipofectamine 2000. (b) *In vivo* luciferase imaging in the solid tumor bearing mice. The photon counts are indicated by the pseudo-color scales. LF 2000, Lipofectamine 2000.

low efficiency of transfection. On the other hand, luciferase expression in the combination of Bubble liposomes and ultrasound was much higher than that in other group (Fig. 5(a)). Koch et al. reported that the combination of ultrasound and microbubble (Levovist) enhanced lipoplex-mediated cell transfection efficiency *in vitro* and also severely damaged most cells. [36]. Therefore, we attempted to confirm the enhancement of transcfection efficiency with Lipofectamine 2000 by Bubble liposomes and ultrasound in the condition without cell damage. The transfection efficiency with lipoplex was not enhanced with Bubble liposomes and ultrasound *in vitro* and *in vivo* (data not shown). The size of Lipofectamine 2000-plasmid DNA complexes was larger than that of naked plasmid DNA by forming the spaghetti–meatball like structure. We guessed that it was difficult for the complexes to enter into cytosol via transient pore on the membrane with cavitation of Bubble liposomes in the condition without cell damage. In the Koch's report, ultrasound was exposed to *in vitro* cells for 60 s with Levovist (20 and 200 mg/mL). In this study, Bubble liposomes (1 mg/mL) were injected into the femoral artery. The concentration of Bubble liposomes would be much lower than that of Levovist because of the dilution of Bubble liposomes in the blood. In addition, the time of ultrasound exposure to Bubble liposomes was very short because of blood flow. Therefore, I thought that the transfection efficiency in the combination of cavitation with Bubble liposomes and lipoplexes was not enhanced. To evaluate gene expression site, we observed luciferase expression with luciferase *in vivo* imaging system (Fig. 5(b)). In the mice treated with Bubble liposomes and ultrasound, luciferase expression was observed in the tumor tissue because of inducing cavitation at ultrasound exposure site. Then, there were a possibility of hemolysis by the cavitation of Bubble liposomes in artery. We examined about hemolytic effect in the treatment of Bubble liposomes and ultrasound (Fig. 6). When the ultrasound was exposed to red blood cell with or without Bubble liposomes *in vitro*, serious hemolysis was not induced. These results suggested that this gene delivery system was important method to achieve tumor specific gene delivery without serious damage.

Plasmid DNA was effectively delivered into S-180 ascites tumor cells and solid tumor tissues with Bubble liposomes and ultrasound, although plasmid DNA did not form a complex with Bubble liposomes because Bubble liposomes were made of neutral charge lipids and modified polyethylene glycol on the surface, and existed free *in vivo*. These results could be explained from Fig. 3. In short, it is thought that Bubble liposomes can immediately and effectively deliver plasmid DNA into cells *in vivo* before the plasmid DNA is degraded by DNase. A mixture of plasmid DNA and Bubble liposomes was injected into mice, and the plasmid DNA was delivered to a specific area of the abdomen or solid tumor tissue by local exposure to ultrasound, suggesting that gene targeting can be induced at a site by exposure to ultrasound. In future studies, we intend to establish minimally-invasive and tissue-specific gene delivery with Bubble liposomes after systemic injection.

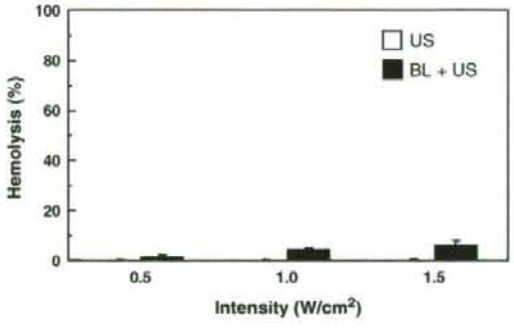

Fig. 6. Hemolysis of red blood cells by Bubble liposomes and ultrasound. Mouse red blood cells (2.5×10^8 cells/ 500 mL) were exposed with ultrasound (frequency: 0.7 MHz, Duty: 50%, Intensity: 0.5–1.5 W/cm^2, Time: 10 s.) in absent or present of Bubble liposomes. Hemolysis was assessed as described in Materials and methods. Each bar represents the mean ± S.D. for triplicate.

The present study showed that Bubble liposomes can be a more effective gene delivery tools into tumor *in vivo* than conventional lipofection. Moreover, Bubble liposomes are an attractive gene delivery approach in cancer gene therapy as the method is minimally-invasive and tumor specific gene transfer, requiring only exposure to ultrasound applied to the surface of the body.

Acknowledgements

We are grateful to Dr. Katsuro Tachibana (Department of Anatomy, School of Medicine, Fukuoka University) for technical advice regarding the induction of cavitation with ultrasound, to Mr. Katsutoshi Kurosawa, Mr. Takamichi Todoroki, Ms. Hitomi Tamagawa (Department of Biopharmaceutics, School of Pharmaceutical Sciences, Teikyo University) for excellent technical assistance, to Dr. Akinori Suginaka (NOF CORPORATION) for technical advice regarding lipids and for providing the lipids, and to Mr. Yasuhiko Hayakawa, Mr. Takahiro Yamauchi and Mr. Kosho Suzuki (NEPA GENE CO., LTD.) for technical advice regarding ultrasound exposure.

This study was supported by an Industrial Technology Research Grant (04A05010) in 2004 from the New Energy and Industrial Technology Development Organization (NEDO) of Japan, a Grant-in-Aid for Young Scientists (160700392, 19700423), Exploratory Research (16650126) from the Japan Society for the Promotion of Science and a Research on Advanced Medical Technology (17070301) in Health and Labour Sciences Research Grants from Ministry of Health, Labour and Welfare.

References

[1] M. Fechheimer, J.F. Boylan, S. Parker, J.E. Sisken, G.L. Patel, S.G. Zimmer, Transfection of mammalian cells with plasmid DNA by scrape loading and sonication loading, Proc. Natl. Acad. Sci. U. S. A. 84 (1987) 8463–8467.

[2] M.W. Miller, D.L. Miller, A.A. Brayman, A review of in vitro bioeffects of inertial ultrasonic cavitation from a mechanistic perspective, Ultrasound Med. Biol. 22 (1996) 1131–1154.

[3] M. Joersbo, J. Brunstedt, Protein synthesis stimulated in sonicated sugar beet cells and protoplasts, Ultrasound Med. Biol. 16 (1990) 719–724.

[4] H.R. Guzman, A.J. McNamara, D.X. Nguyen, M.R. Prausnitz, Bioeffects caused by changes in acoustic cavitation bubble density and cell concentration: a unified explanation based on cell-to-bubble ratio and blast radius, Ultrasound Med. Biol. 29 (2003) 1211–1222.

[5] D.L. Miller, S.V. Pislaru, J.E. Greenleaf, Sonoporation: mechanical DNA delivery by ultrasonic cavitation, Somat. Cell Mol. Genet. 27 (2002) 115–134.

[6] W. Wei, B. Zheng-zhong, W. Yong-jie, Z. Qing-wu, M. Ya-lin, Bioeffects of low-frequency ultrasonic gene delivery and safety on cell membrane permeability control, J. Ultrasound. Med. 23 (2004) 1569–1582.

[7] M. Duvshani-Eshet, M. Machluf, Therapeutic ultrasound optimization for gene delivery: a key factor achieving nuclear DNA localization, J. Control Release 108 (2005) 513–528.

[8] H.J. Kim, J.F. Greenleaf, R.R. Kinnick, J.T. Bronk, M.E. Bolander, Ultrasound-mediated transfection of mammalian cells, Hum. Gene Ther. 7 (1996) 1339–1346.

[9] D.B. Tata, F. Dunn, D.J. Tindall, Selective clinical ultrasound signals mediate differential gene transfer and expression in two human prostate cancer cell lines: LnCap and PC-3, Biochem. Biophys. Res. Commun. 234 (1997) 64–67.

[10] W.J. Greenleaf, M.E. Bolander, G. Sarkar, M.B. Goldring, J.F. Greenleaf, Artificial cavitation nuclei significantly enhance acoustically induced cell transfection, Ultrasound Med. Biol. 24 (1998) 587–595.

[11] T. Li, K. Tachibana, M. Kuroki, M. Kuroki, Gene transfer with echo-enhanced contrast agents: comparison between Albunex, Optison, and Levovist in mice-initial results, Radiology 229 (2003) 423–428.

[12] R.V. Shohet, S. Chen, Y.T. Zhou, Z. Wang, R.S. Meidell, R.H. Unger, P.A. Grayburn, Echocardiographic destruction of albumin microbubbles directs gene delivery to the myocardium, Circulation 101 (2000) 2554–2556.

[13] S. Sonoda, K. Tachibana, E. Uchino, A. Okubo, M. Yamamoto, K. Sakoda, T. Hisatomi, K.H. Sonoda, Y. Negishi, Y. Izumi, S. Takao, T. Sakamoto, Gene transfer to corneal epithelium and keratocytes mediated by ultrasound with microbubbles, Investig. Ophthalmol. Vis. Sci. 47 (2006) 558–564.

[14] Y. Taniyama, K. Tachibana, K. Hiraoka, M. Aoki, S. Yamamoto, K. Matsumoto, T. Nakamura, T. Ogihara, Y. Kaneda, R. Morishita, Development of safe and efficient novel nonviral gene transfer using ultrasound: enhancement of transfection efficiency of naked plasmid DNA in skeletal muscle, Gene Ther. 9 (2002) 372–380.

[15] Y. Taniyama, K. Tachibana, K. Hiraoka, T. Namba, K. Yamasaki, N. Hashiya, M. Aoki, T. Ogihara, K. Yasufumi, R. Morishita, Local delivery of plasmid DNA into rat carotid artery using ultrasound, Circulation 105 (2002) 1233–1239.

[16] J.R. Lindner, Microbubbles in medical imaging: current applications and future directions, Nat. Rev. Drug Discov. 3 (2004) 527–532.

[17] S. Tsunoda, O. Mazda, Y. Oda, Y. Iida, S. Akabame, T. Kishida, M. Shin-Ya, H. Asada, S. Gojo, J. Imanishi, H. Matsubara, T. Yoshikawa, Sonoporation using microbubble BR14 promotes pDNA/siRNA transduction to murine heart, Biochem. Biophys. Res. Commun. 336 (2005) 118–127.

[18] M. Harata, Y. Soda, K. Tani, J. Ooi, T. Takizawa, M. Chen, Y. Bai, K. Izawa, S. Kobayashi, A. Tomonari, F. Nagamura, S. Takahashi, K. Uchimaru, T. Iseki, T. Tsuji, T.A. Takahashi, K. Sugita, S. Nakazawa, A. Tojo, K. Maruyama, S. Asano, CD19-targeting liposomes containing imatinib efficiently kill Philadelphia chromosome-positive acute lymphoblastic leukemia cells, Blood 104 (2004) 1442–1449.

[19] O. Ishida, K. Maruyama, H. Tanahashi, M. Iwatsuru, K. Sasaki, M. Eriguchi, H. Yanagie, Liposomes bearing polyethyleneglycol-coupled transferrin with intracellular targeting property to the solid tumors in vivo, Pharm. Res. 18 (2001) 1042–1048.

[20] K. Kawamura, N. Kadowaki, R. Suzuki, S. Udagawa, S. Kasaoka, N. Utoguchi, T. Kitawaki, N. Sugimoto, N. Okada, K. Maruyama, T. Uchiyama, Dendritic cells that endocytosed antigen-containing IgG-liposomes elicit effective antitumor immunity, J. Immunother. 29 (2006) 165–174.

[21] K. Maruyama, E. Holmberg, S.J. Kennel, A. Klibanov, V.P. Torchilin, L. Huang, Characterization of in vivo immunoliposome targeting to pulmonary endothelium, J. Pharm. Sci. 79 (1990) 978–984.

[22] K. Maruyama, O. Ishida, S. Kasaoka, T. Takizawa, N. Utoguchi, A. Shinohara, M. Chiba, H. Kobayashi, M. Eriguchi, H. Yanagie, Intracellular targeting of sodium mercaptoundecahydrododecaborate (BSH) to solid tumors by transferrin-PEG liposomes, for boron neutron-capture therapy (BNCT), J. Control. Release 98 (2004) 195–207.

[23] K. Maruyama, S.J. Kennel, L. Huang, Lipid composition is important for highly efficient target binding and retention of immunoliposomes, Proc. Natl. Acad. Sci. U. S. A. 87 (1990) 5744–5748.

[24] H. Yanagie, K. Maruyama, T. Takizawa, O. Ishida, K. Ogura, T. Matsumoto, Y. Sakurai, T. Kobayashi, A. Shinohara, J. Rant, J. Skvarc, R. Ilic, G. Kuhne, M. Chiba, Y. Furuya, H. Sugiyama, T. Hisa, K. Ono, H. Kobayashi, M. Eriguchi, Application of boron-entrapped stealth liposomes to inhibition of growth of tumour cells in the in vivo boron neutron-capture therapy model, Biomed. Pharmacother. 60 (2006) 43–50.

[25] H. Yanagie, K. Ogura, K. Takagi, K. Maruyama, T. Matsumoto, Y. Sakurai, J. Skvarc, R. Illic, G. Kuhne, T. Hisa, I. Yoshizaki, K. Kono, Y. Furuya, H. Sugiyama, H. Kobayashi, K. Ono, K. Nakagawa, M. Eriguchi, Accumulation of boron compounds to tumor with polyethylene-glycol binding liposome by using neutron capture autoradiography, Appl. Radiat. Isotopes 61 (2004) 639–646.

[26] H. Hatakeyama, H. Akita, K. Kogure, M. Oishi, Y. Nagasaki, Y. Kihira, M. Ueno, H. Kobayashi, H. Kikuchi, H. Harashima, Development of a novel

systemic gene delivery system for cancer therapy with a tumor-specific cleavable PEG-lipid, Gene Ther. 14 (2007) 68–77.

[27] R. Suzuki, T. Takizawa, Y. Negishi, K. Hagisawa, K. Tanaka, K. Sawamura, N. Utoguchi, T. Nishioka, K. Maruyama, Gene delivery by combination of novel liposomal bubbles with perfluoropropane and ultrasound, J. Control. Release 117 (2007) 130–136.

[28] H. Mizuguchi, T. Nakagawa, M. Nakanishi, S. Imazu, S. Nakagawa, T. Mayumi, Efficient gene transfer into mammalian cells using fusogenic liposome, Biochem. Biophys. Res. Commun. 218 (1996) 402–407.

[29] K. Kono, Y. Torikoshi, M. Mitsutomi, T. Itoh, N. Emi, H. Yanagie, T. Takagishi, Novel gene delivery systems: complexes of fusigenic polymer-modified liposomes and lipoplexes, Gene Ther. 8 (2001) 5–12.

[30] N. Sakaguchi, C. Kojima, A. Harada, K. Koiwai, K. Shimizu, N. Emi, K. Kono, Enhancement of transfection activity of lipoplexes by complexation with transferrin-bearing fusogenic polymer-modified liposomes, Int. J. Pharm. 325 (2006) 186–190.

[31] T. Kakudo, S. Chaki, S. Futaki, I. Nakase, K. Akaji, T. Kawakami, K. Maruyama, H. Kamiya, H. Harashima, Transferrin-modified liposomes equipped with a pH-sensitive fusogenic peptide: an artificial viral-like delivery system, Biochemistry 43 (2004) 5618–5628.

[32] M. Kondoh, T. Matsuyama, R. Suzuki, H. Mizuguchi, T. Nakanishi, S. Nakagawa, Y. Tsutsumi, M. Nakanishi, M. Sato, T. Mayumi, Growth inhibition of human leukemia HL-60 cells by an antisense phosphodiester oligonucleotide encapsulated into fusogenic liposomes, Biol. Pharm. Bull. 23 (2000) 1011–1013.

[33] H. Leong-Poi, J. Christiansen, A.L. Klibanov, S. Kaul, J.R. Lindner, Noninvasive assessment of angiogenesis by ultrasound and microbubbles targeted to alpha(v)-integrins, Circulation 107 (2003) 455–460.

[34] M. Takahashi, K. Kido, A. Aoi, H. Furukawa, M. Ono, T. Kodama, Spinal gene transfer using ultrasound and microbubbles, J. Control. Release 117 (2007) 267–272.

[35] H. Mizuguchi, T. Nakagawa, S. Toyosawa, M. Nakanishi, S. Imazu, T. Nakanishi, Y. Tsutsumi, S. Nakagawa, T. Hayakawa, N. Ijuhin, T. Mayumi, Tumor necrosis factor alpha-mediated tumor regression by the in vivo transfer of genes into the artery that leads to tumors, Cancer Res. 58 (1998) 5725–5730.

[36] S. Koch, P. Pohl, U. Cobet, N.G. Rainov, Ultrasound enhancement of liposome-mediated cell transfection is caused by cavitation effects, Ultrasound Med. Biol. 26 (2000) 897–903.

Low-intensity ultrasound and microbubbles enhance the antitumor effect of cisplatin

Yukiko Watanabe,[1] Atsuko Aoi,[2] Sachiko Horie,[1] Noriko Tomita,[1] Shiro Mori,[3] Hidehiro Morikawa,[3] Yasuhiro Matsumura,[4] Georges Vassaux[5,6] and Tetsuya Kodama[1,7]

[1]Graduate School of Biomedical Engineering, [2]Graduate School of Dentistry, Tohoku University, [3]Tohoku University Hospital, Sendai, Miyagi 980-8575; [4]Investigative Treatment Division, Research Center for Innovative Oncology, National Cancer Center Hospital East, Kashiwa, Chiba 277-8577, Japan; [5]CIC-INSERM 00-04, EA 4274, CHU Hôtel Dieu, Nantes, cedex 1; [6]Institut des Maladies de l'Appareil Digestif, CHU Hotel Dieu, Nantes, cedex 1, France

(Received July 18, 2008/Revised August 21, 2008/Accepted August 24, 2008/Online publication November 19, 2008)

Cell permeabilization using microbubbles (MB) and low-intensity ultrasound (US) have the potential for delivering molecules into the cytoplasm. The collapsing MB and cavitation bubbles created by this collapse generate impulsive pressures that cause transient membrane permeability, allowing exogenous molecules to enter the cells. To evaluate this methodology *in vitro* and *in vivo*, we investigated the effects of low-intensity 1-MHz pulsed US and MB combined with *cis*-diamminedichloroplatinum (II) (CDDP) on two cell lines (Colon 26 murine colon carcinoma and EMT6 murine mammary carcinoma) *in vitro* and *in vivo* on severe combined immunodeficient mice inoculated with HT29-luc human colon carcinoma. To investigate *in vitro* the efficiency of molecular delivery by the US and MB method, calcein molecules with a molecular weight in the same range as that of CDDP were used as fluorescent markers. Fluorescence measurement revealed that approximately 10^6–10^7 calcein molecules per cell were internalized. US–MB-mediated delivery of CDDP in Colon 26 and EMT6 cells increased cytotoxicity in a dose-dependent manner and induced apoptosis (nuclear condensation and fragmentation, and increase in caspase-3 activity). *In vivo* experiments with xenografts (HT29-luc) revealed a very significant reduction in tumor volume in mice treated with CDDP + US + MB compared with those in the US + CDDP groups for two different concentrations of CDDP. This finding suggests that the US–MB method combined with chemotherapy has clinical potential in cancer therapy. (*Cancer Sci* 2008; 99: 2525–2531)

Microbubbles (MB) have been developed as ultrasound (US) contrast agents with a diameter of less than 10 μm. The components of their shell membrane vary (albumin, lipid, or polymer), and gases such as air or perfluorocarbons are internalized in them.[1–3] These bubbles oscillate non-linearly in an US field and emit harmonic and subharmonic acoustic signals, thereby enabling differentiation between acoustic scattering and vascular signatures. In addition, because these bubbles behave similar to red blood cells, they have been used to evaluate the blood pool and blood flow at the microvascular level.[4]

Microbubbles collapse in the presence of low-intensity US. There is evidence that impulsive pressures generated by either collapsing MB[5,6] or the cavitation bubbles created by this collapse may permeabilize the plasma membrane of neighboring cells.[7,8] This process results in the diffusion of nearby exogenous molecules into the cytoplasm and a subsequent biological response.[8–11] Because these impulsive pressures can be induced by high-intensity US,[12,13] substantial thermal and mechanical side effects can be reduced using the US–MB method.

The US–MB method is non-toxic and non-immunogenic, and allows local or systemic administration. This method can be used to deliver exogenous molecules into dividing and non-dividing cells and has been investigated as an approach for *in vivo* gene transfer and molecular delivery.[14–16] In any case, the efficiency of molecular delivery depends on the size of the molecules to be delivered.[17,18] The amount of molecules increases with decreasing molecular weight. Thus, it is expected that this methodology will be useful for therapeutic strategies involving drugs with small molecular sizes. Cis-diamminedichloroplatinum (II) (cisplatin; CDDP) is one of the most effective and commonly used chemotherapeutics, possessing a molecular weight of 300. CDDP has been used for the treatment of many solid tumors, including those of the ovaries, testicles, bladder, lung, and head and neck.[19] Increasing CDDP penetration into the tumor cells could further improve its therapeutic efficacy. In the present study, we estimated the number of CDDP molecules internalized by the US–MB method using calcein molecules with molecular weights in the same range as that of CDDP as fluorescent markers. Subsequently, we assessed the therapeutic potential of the combination of CDDP and US with MB *in vitro* and *in vivo* and demonstrated that this combination induces apoptotic effects, and increases the therapeutic efficacy.

Materials and Methods

In vitro and *in vivo* studies were carried out in accordance with the ethical guidelines approved by Tohoku University.

Cell preparation. Human embryonic kidney (293T) cells were a generous gift from Dr Ono of Tohoku University. Murine mammary carcinoma (EMT6) cells were obtained from the American Type Culture Collection (Rockville, MD, USA). Murine colon carcinoma (Colon 26) cells were obtained from the Cell Resource Center for Biomedical Research of the Institute of Development, Aging and Cancer, Tohoku University (Sendai, Japan). Human colon carcinoma (HT-29-luc) cells stably transfected with a plasmid carrying the firefly luciferase gene driven by a cytomegalovirus promoter were obtained from Xenogen (Alameda, CA, USA). Colon 26 and HT-29-luc cells were cultured under standard conditions in RPMI-1640 medium supplemented with 10% heat-inactivated fetal bovine serum (Invitrogen, Carlsbad, CA, USA) and 1% L-glutamine–penicillin–streptomycin (Sigma-Aldrich, St Louis, MO, USA), whereas 293T and EMT6 cells were cultured in Dulbecco's modified Eagle's medium (Sigma-Aldrich) containing the same supplements as those added to the RPMI-1640 medium. HT29-luc cells were selected in 1 mg/mL geneticin (G418) (Sigma-Aldrich). Cells cultured in a 10-cm culture dish were maintained in a humidified incubator at 37°C under an atmosphere containing 5% CO_2 and

[7]To whom correspondence should be addressed.
E-mail: kodama@bme.tohoku.ac.jp

doi: 10.1111/j.1349-7006.2008.00989.x

95% air. The total cell counts and viability were counted in a hemocytometer by the trypan blue dye exclusion method[20] prior to US exposure. Only cells in their exponential growth phase with a viability ≥99% were used for the study.

Microbubbles. MB were created in an aqueous dispersion of 2 mg/mL 1,2-distearoyl-sn-glycero-3-phosphocholine (Avanti Polar Lipids, Alabaster, AL, USA) and 1 mg/mL polyethylene glycol 40 stearate (Sigma-Aldrich) using a 20-kHz sonicator (Vibra Cell; Sonics and Materials, Danbury, CT, USA) in the presence of C_3F_8 gas.[21] The lipid molecules that formed components of the MB surface were confirmed by staining the molecules with 3 μmol/L FM1-43 (excitation 479 nm, emission 598 nm; Molecular Probes, Eugene, OR, USA) and observing them under an inverted microscope (IX81; Olympus, Tokyo, Japan). The peak diameter and the zeta potential of the MB were determined to be 1272 ± 163 nm ($n = 7$) and –4.1 ± 0.85 mV ($n = 3$), respectively, by using a laser diffraction particle size analyzer (particle range 0.6 nm–7 μm; ELSZ-2; Otsuka Electronics, Osaka, Japan).

Ultrasound exposure. Three 1-MHz submersible US probes were used. A 12-mm (Fuji Ceramics, Fujinomiya, Japan) and a 30-mm diameter probe (BFC Applications, Fujisawa, Japan) were used for the *in vitro* experiments, whereas 38-mm diameter probes (Fuji Ceramics) were used for the *in vivo* experiments. Each probe was placed in the test chamber (380 mm × 250 mm × 130 mm) that was previously filled with tap water. Signals of 1 MHz were generated by a multifunction synthesizer (WF1946A; NF Co., Yokohama, Japan) and amplified with a high-speed bipolar amplifier (HSA4101; NF Co.). The pressure values were measured using a polyvinylidene fluoride (PVDF) needle hydrophone (PVDF-Z44-1000; Specialty Engineering Associates, Soquel, CA, USA) at a stand-off distance of 1 mm from the transducer surface by using a stage control system (Mark-204-MS; Sigma Koki, Tokyo, Japan). The signals from both the amplifier and the hydrophone were recorded onto a digital phosphor oscilloscope (Wave Surfer 454, 500 MHz, 1 MΩ [16 pF]; LeCroy Co., Chestnut, NY, USA) in top water degassed with transducer (SPN-620) generated by ultrasonic generator α2 (GP-622D) (Tiyoda Electric Co., Chikuma, Japan). The positive and negative peak values of the pressures were the same. Two intensities, 0.5 and 1.0 W/cm^2, were used in the *in vitro* experiments. The duty cycle was 50%, the number of pulses was 2000, the pulse repletion frequency was 250 Hz, and the exposure time was 10 s. For the *in vivo* experiments, the intensity was 3.0 W/cm^2, the duty cycle was 20%, the number of pulses was 200; the pulse repletion frequency was 1000 Hz, and the exposure time was 60 s. The intensity was defined as the average rate of flow of energy through a unit area placed normal to the direction of propagation.

***In vitro* quantization of calcein uptake.** The 293T cells (5×10^4 cells/well) were seeded in complete medium onto 48-well plates and incubated at 37°C in a 5% CO_2 incubator. On the next day, the medium was replaced with fresh medium containing 200 μmol/L calcein (molecular weight 622) (excitation 494 nm, emission 517 nm; Sigma-Aldrich) with and without MB (10% v/v). After US exposure for 10 s, the cells were washed with phosphate-buffered saline (PBS), trypsinized, and collected in a 15-mL conical tube. Thereafter, the cells were washed three times and transferred to a 1.5-mL conical tube in which they were pelleted. The pellets were lysed in 200 μL reporter lysis buffer (Promega, Madison, WI, USA) and subsequently frozen at –80°C for 15 min. The cells were thawed on ice. Each cell lysate was centrifuged at 12 000*g* for 2 min to pellet the cell debris. Twenty microliters of the supernatant was examined for the uptake of fluorescent molecules using Mx3000P software (Stratagene, La Jolla, CA, USA). The fluorescence of these molecules was excited using a quartz tungsten halogen lamp (350–750 nm), and the emission was collected with a 492–516-nm bandpass filter. The fluorescence data were analyzed with MxPro QPCR Software (Stratagene). The total protein content from an aliquot of each sample of supernatant was calculated by establishing albumin standard curves (BCA protein assay kit; Pierce, Rockford, IL, USA). In addition, two other standard curves were utilized: one to determine the total protein content of the cells, and the other to determine the concentration and intensity of the fluorescence. The experiment was carried out with samples and standards in duplicate, and the absorption of the protein was measured at 562 nm using a plate reader (Sunrise; Tecan Austria, Salzburg, Austria) with the data analysis software LS-Plate manager RD 2001 (Win) (Sunrise). The number of equivalent fluorescent molecules per cell was determined from the calibration curves.

Imaging of confocal fluorescence microscopy. The 293T cells (5×10^4 cells/well) were seeded in complete medium onto alternate 48-well plates to prevent US exposure of neighboring cells.[8] On the next day, the medium was replaced with fresh medium (110 μL) containing calcein (200 μmol/L) with and without MB (10% v/v). After US exposure of 10 s, the plates were incubated for 24 h. Thereafter, the cells were washed three times with PBS and trypsinized. Finally, the cell pellet was resuspended in 60 μL propidium iodide (PI) (excitation 536 nm, emission 617 nm; Molecular Probes) (0.7 μg/mL) and incubated at room temperature for 10–15 min. The calcein and PI fluorescence intensities were determined with a confocal microscope (FV1000; Olympus). A ×60 oil-immersion objective lens with a numerical aperture of 1.25 was used. Calcein and PI fluorescence were excited with the 488-nm line of an argon laser. The laser excitation beam was directed to the specimen through a 488-nm dichroic beam splitter. The emitted fluorescence was collected through a 510–550-nm bandpass emission filter in the green channel and a 580-nm longpass filter in the red channel. Computer-generated images of 1-μm optical sections were obtained at the approximate geometric center of the cell as determined by repeated optical sectioning.

***In vitro* delivery of CDDP.** CDDP (molecular weight 300) was donated by Nihon Kayaku (Tokyo, Japan). Colon 26 and EMT6 cells were seeded in complete medium onto 10-cm culture dishes. Both cells were trypsinized, counted, and transferred into 15-mL round tubes at concentrations of 5×10^5 and 3×10^5 cells/mL, respectively. For control samples, 1 mL complete medium was used as the sample solution; for treated samples, the sample solution was mixed with 800 μL complete medium, 100 μL CDDP solution (0.5–1.0 mmol/L), and 100 μL MB solution (7% v/v). Each tube was positioned above a 30-mm diameter US probe that was immersed in tap water and exposed to US (10 s; 0.5 W/cm^2). After exposure, 4 mL PBS was added to each tube and centrifuged for 5 min at 4°C (350*g*). The cells were washed twice with PBS and subsequently seeded in 1 mL complete medium onto 24-well plates. The plates were incubated for 24 h at 37°C in a 5% CO_2 incubator. The cell viability was determined by a 3-(4,5-dimethylthiazol-2-yl)-2, 5-diphenyltetrazolium bromide (MTT) assay as described previously.[22] Each experiment was carried out with five samples. For each experiment, the mean percentage of treated samples was divided by the mean percentage of control samples to obtain the survival fraction. The mean of five survival fractions was calculated for each condition. The survival fraction of each cell line was measured at the CDDP concentration at which the highest statistical significance was obtained.

***In vitro* analysis of apoptosis.** Colon 26 (5×10^4 cells/well) cells were seeded onto alternate 48 wells to prevent the US exposure of neighboring cells.[8] The medium was replaced with fresh medium (110 μL) containing CDDP (1.5 mg) with and without MB (7% v/v). After US exposure, the plates were incubated for 1 h in a 5% CO_2 incubator, supplemented with 390 μL complete medium; subsequently, the plates were incubated for an additional 24 h at 37°C in the same incubator. The final

doi: 10.1111/j.1349-7006.2008.00989.x

concentration of CDDP was 10 μmol/L. The cell viability was determined by an MTT assay as described previously.[22] Staining with 4′,6-diamidino-2-phenylindole (DAPI; Sigma-Aldrich) was carried out for observing nuclear condensation and fragmentation. Twenty-four hours after the addition of CDDP, the cells were washed with PBS, stained with 100 μL DAPI (100 ng/mL) solution, and observed under an inverted microscope (IX 81). DAPI fluorescence of the cell nuclei was visualized by excitation at 330–385 nm with a 420-nm barrier filter. For determining the induction of apoptotic mediator proteins, caspase-3 activity was measured using a colorimetric assay kit (Medical and Biological Laboratories, Woburn, MA, USA) 24 h after the treatment. In brief, the treated cells were collected from 12 wells of the 48-well plates and suspended in cell lysis buffer. Aliquots of protein were incubated in a reaction buffer containing 10 mmol/L dithiothreitol (DTT) at 37°C for 1 h. A p-nitroaniline-conjugated synthetic peptide was used as the substrate. The caspase activity was calculated by measuring the optic absorbance at 400 nm using a plate reader with the data analysis software LS-Plate manager RD 2001 (Win).

***In vivo* therapeutic effects.** To evaluate the antitumor effects of MB, the antitumor effects of CDDP + US and CDDP + US + MB were compared using xenografts of HT29-luc cells. Two CDDP concentrations (0.5 and 1.25 μg/g bodyweight) were used. HT29-luc cells (1×10^6 cells) in 100 μL saline were injected subcutaneously into the right and left flanks of 16 male severe combined immunodeficient mice aged 6–9 weeks (mouse bodyweight was set to 20 g). The mice were assigned randomly into two groups. On days 3, 7, and 10, all mice were injected intratumorally with the following assigned treatments. (i) Four mice received 20 μL CDDP (0.5 μg/μL bodyweight) with 80 μL saline per site following US exposure (CDDP + US), and four others received 20 μL CDDP (0.5 μg/μL bodyweight) with 30 μL saline and 50 μL MB per site following US exposure (CDDP + US + MB). (ii) Four mice received 50 μL CDDP (1.25 μg/μL bodyweight) with 50 μL saline per site following US exposure (CDDP + US), and four others received 50 μL CDDP (1.25 μg/μL bodyweight) with 50 μL MB per site following US exposure (CDDP + US + MB). The tumors were immersed in tap water with a temperature of 37°C, positioned just above the 38-mm diameter US probe, and exposed to US (3.0 W/cm^2, 60 s). Bioluminescence induced by CDDP + US + MB was normalized with that of CDDP + US at each concentration (0.5 and 1.25 μg/g bodyweight) on days 4, 7, 9, and 11 to provide the antitumor effects of MB.

Bioluminescence imaging. On days 4, 7, 9, and 11, the mice were anesthetized with isoflurane. Subsequently, they were injected intraperitoneally with luciferin (150 μg/g bodyweight) and placed on the *in vivo* imaging system (IVIS100; Xenogen). The bioluminescence signals were monitored at 10-s time intervals after 10 min luciferin administration. The signal intensity was quantified as the sum of all detected photon counts within the region of interest after subtraction of the measured background luminescence. The light intensity closely correlated with the tumor volume (EMT6-luc) up to 100 mm^3, at which point the tumor volume was calculated according to the formula $(\pi/6) \times (\text{width})^2 \times (\text{length})$.[21] In the present experiment, all tumors (HT29-luc) with a volume less than 100 mm^3 were subjected to treatment.

Statistical analysis. All measurements are expressed as mean ± SEM. An overall difference between the groups was determined by one-way analysis of variance (one-way ANOVA). When the one-way ANOVA results were significant for three samples, the differences between each group were estimated using the Tukey–Kramer test. Simple comparisons of the mean and SEM of the data were carried out using Student's *t*-test. The differences were considered to be significant at $P < 0.05$.

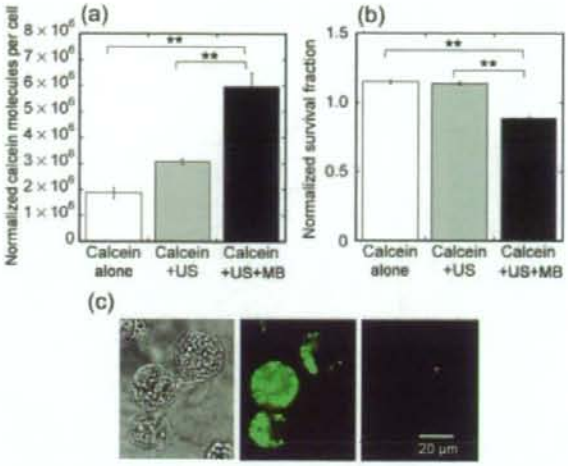

Fig. 1. Uptake of fluorescent molecules by 293T cells. (a) Mean fluorescence uptake under various conditions (calcein alone, calcein + ultrasound [US], and calcein + US + microbubbles [MB]). The calcein + US + MB condition results in a significant increase in the uptake of fluorescent molecules (6.0 ± 0.5 ¥ 106 molecules per cell) compared to calcein alone and calcein + US. Calcein alone (n = 4), calcein + US (n = 4), calcein + US + MB (n = 4). (b) Cell viability measured by the a 3-(4,5-dimethylthiazol-2-yl)-2, 5-diphenyltetrazolium bromide (MTT) assay. The survival fraction is decreased slightly by the effect of US + MB. Calcein alone (n = 4), calcein + US (n = 4), calcein + US + MB (n = 4). (c) Confocal microscopy showing differential interference contrast (left) and fluorescence images (middle) or representative viable 293T cells (right) exposed to US in the presence of MB. Propidium iodide (PI) staining was carried out with fluorescence staining in some cases to confirm that the cells that acquired calcein were viable and excluded PI. Scale bars = 20 mm. Ultrasound intensity 1.0 W/cm2; duty cycle 50%; number of pulses 2000; pulse repletion frequency 250 Hz; and exposure time 10 s. **P < 0.01.

Results

Uptake of fluorescent molecules. Calcein, which has a molecular weight of 622 (calculated stokes radius of 0.68),[23] was used as a fluorescent marker to evaluate small-molecule entry in cancer cells upon US–MB stimulation. As the molecular weight of CDDP is 300 (calculated stokes radius is 0.48 nm), calcein can be considered to represent a realistic marker of CDDP entry into tumor cells.

The exposure of cells to US in the presence of MB resulted in the delivery of 10^6–10^7 calcein molecules per cell (Fig. 1a). This represents a significant increase in the uptake of fluorescent molecules compared to calcein alone and calcein + US. Figure 1b shows that this effect was achieved with a very limited loss of cell viability that was measured by MTT assay, where the survival fraction rate due to MB alone was not investigated as it was found that MB alone did not contribute to cell viability.[24] To confirm that the calcein molecules actually entered the cytoplasm, confocal fluorescence microscopic analysis was carried out. Figure 1c shows the differential interference contrast and fluorescence images or the representative viable 293T cells exposed to US in the presence of MB. PI staining was also carried out with some instances of fluorescence staining to confirm that the cells that acquired calcein were viable and excluded PI. Some cells treated with US in the presence of MB demonstrated intense fluorescence distributed uniformly throughout the entire cell, whereas other cells demonstrated localized intense fluorescence (Fig. 1c).

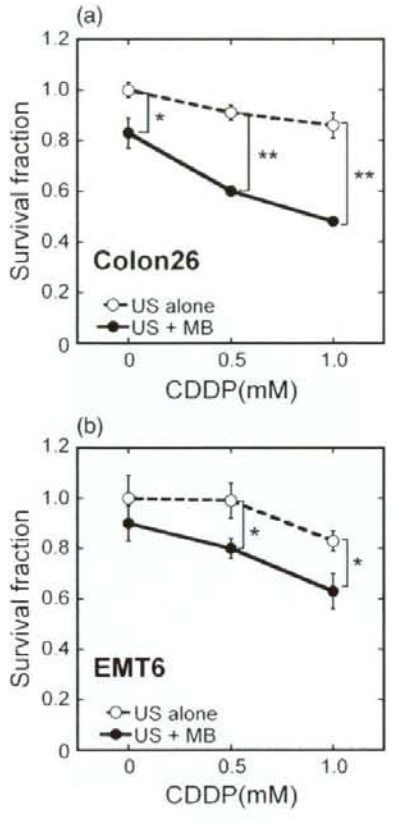

Fig. 2. Potentiation of in vitro cis-diamminedichloroplatinum (II) (CDDP) cytotoxicity in Colon 26 and EMT6 cells. (a) Colon 26: (s) ultrasound (US) alone (n = 5) and (d) US + microbubbles (MB) (n = 5). (b) EMT6: (s) US alone (n = 5) and (d) US + MB (n = 5). Cell survival was measured by a 3-(4,5-dimethylthiazol-2-yl)-2, 5-diphenyltetrazolium bromide (MTT) assay 24 h after US exposure. US intensity 0.5 W/cm2; duty cycle 50%; number of pulses 2000; pulse repletion frequency 250 Hz; and exposure time 10 s. The bars represent mean ± SEM. *P < 0.05, **P < 0.01.

Cytotoxicity *in vitro*. The cytotoxicity of various doses of CDDP in the presence of US with and without MB was tested on Colon 26 and EMT6 cells (Fig. 2). A marked increase in CDDP toxicity was observed under the US–MB conditions, whereas US alone did not significantly affect cell survival with various CDDP concentrations. The CDDP toxicity depended slightly on the cell type.

Apoptosis assay. CDDP is known to induce apoptosis.[25] We confirmed the involvement of apoptosis in mediating cytotoxicity in response to CDDP. Cells undergoing apoptosis demonstrate characteristic nuclear morphological changes with DAPI staining. Figure 3 shows phase contrast and DAPI images of Colon 26 cells. Untreated control cells (Fig. 3a,b) and cells treated with US + MB (Fig. 3c,d), CDDP alone (Fig. 3e,f), and CDDP + US (Fig. 3g,h) showed extremely little condensed or fragmented chromatin. The majority of cells treated with CDDP + US + MB (Fig. 3i,j) displayed apoptotic features, including condensed nuclei and nuclear fragmentation.

Induction of caspase-3 has been suggested as a marker of apoptosis.[26] Figure 4 shows that treatment with US + MB activates caspase-3 as compared to treatment with CDDP alone or with CDDP + US. The caspase activity increases with time. Taken together, the data presented in Figures 3 and 4 demonstrate that the CDDP + US + MB combination decreases cell viability and that this reduction in cell survival is associated with increased induction of apoptosis. In the present study, we did not consider the activation of caspase-3 by US because US alone did not contribute to the survival fraction (Fig. 2) and subsequent apoptosis induction (Fig. 3).

***In vivo* therapeutic effects of MB.** From the above *in vitro* experiments, we found that MB associated with US are able to trigger the uptake of small molecules (Fig. 1), thereby inducing antitumor effects (Fig. 2) and apoptosis (Figs 3,4) in conjunction with CDDP. Thereafter, we investigated the *in vivo* antitumor effects of using MB, in cases in which the xenografts of HT29-luc cells were used. We investigated the antitumor effects of CDDP + US + MB on the xenografts with two different CDDP concentrations (0.5 and 1.25 μg/g bodyweight) on days 4, 7, 9, and 11. The luciferase activity for each concentration of CDDP + US + MB was normalized with each concentration of CDDP + US that was administered previously (Fig. 5a) in order to determine the antitumor effects of MB alone. The activities of the MB were recognized after day 7 (second treatment) in both groups. On day 11, a significant reduction was observed in the CDDP + US + MB group compared to the control and US + MB

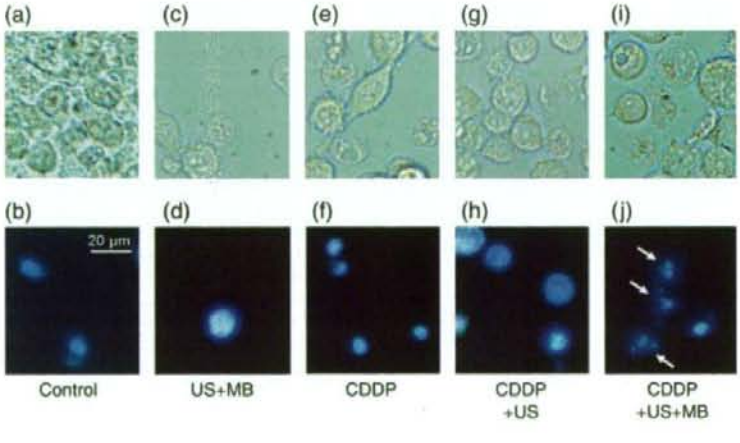

Fig. 3. Nuclear condensation and fragmentation. (a,c,e,g,i) Differential interference contrast and (b,d,f,h,j) 4′,6-diamidino-2-phenylindole (DAPI) fluorescence images of representative viable Colon 26 cells 24 h after treatment. 10 μmol/L cis-diamminedichloroplatinum (II) (CDDP): (a,b) control, (c,d) ultrasound (US) + microbubbles (MB), (e,f) CDDP, (g,h) CDDP + US, and (i,j) CDDP + US + MB. Round or shrunken nuclei of DAPI-stained cells (white arrows) are hallmarks of apoptosis in (j). Experiments were repeated three times with similar results. Scale bar = 20 μm. Ultrasound intensity 1.0 W/cm^2; duty cycle 50%; number of pulses 2000; pulse repletion frequency 250 Hz; and exposure time 10 s.

doi: 10.1111/j.1349-7006.2008.00989.x